

DEPARTMENT OF THE INTERIOR  
U.S. GEOLOGICAL SURVEY

Processing of the GLIMPCE  
Multichannel Seismic Data

By

M.W. Lee<sup>1</sup>, W.F. Agena<sup>1</sup>, and D.R. Hutchinson<sup>2</sup>

U.S. Geological Survey  
Open-File Report 88-225

This report is preliminary and has not been reviewed for conformity with U.S. Geological Survey editorial standards and stratigraphic nomenclature. Any use of trade names is for descriptive purposes only and does not imply endorsement by the U.S. Geological Survey.

<sup>1</sup>U.S. Geological Survey, Box 25046, Denver Federal Center, Denver, CO 80225

<sup>2</sup>U.S. Geological Survey, Building B, Quissett Campus, Woods Hole, MA 02543

## TABLE OF CONTENTS

	Page
Abstract.....	1
Introduction.....	1
Acknowledgment.....	3
Data acquisition.....	3
Preparation.....	5
Processing phase 1A.....	5
Analysis of coherent noise.....	12
Processing phase 1B.....	19
Post-stack processing techniques.....	25
Results and discussion.....	27
Conclusions.....	27
References.....	32
Appendix A.....	33
Appendix B.....	38

## ILLUSTRATIONS

Figure 1. Location of GLIMPCE seismic reflection profiles.....	2
2. Processing flow chart for GLIMPCE seismic data.....	7
3. Example of stacked seismic section with 12.5 m CDP interval.....	10
4. Amplitude response of 4 trace vertical stack operator.....	11
5. Final stacked section with 50 m CDP interval.....	13
6. Out-of-plane side-scattering noise and its F-K analysis...	14
7. In-line side-scattering noise and its F-K analysis.....	16
8. Examples of shot gather showing strong multiples.....	17
9. Result of spiking deconvolution.....	18
10. Example of shot domain F-K filtering.....	20
11. Detailed computer implementation on water-bottom multiple suppression.....	21
12. Example of stacked section with 12.5 m CDP interval.....	23
13. Final stacked section with 50-m CDP interval.....	24
14. The result of post-stack amplitude enhancement.....	26
15. Final stacked profile for line A showing Moho and Archean basement.....	28
16-18. Comparison between phase 1A and phase 1B data processing: for upper 0-5 seconds near shot point 1500 of line A.....	29
for middle 5-10 seconds near shot point 2500 of line A.....	30
for lower 10-15 seconds near shot point 500 of line A.....	31

## TABLES

Table 1. Summary of GLIMPCE seismic lines.....	4
2. Recording parameters.....	6

## PROCESSING OF THE GLIMPCE MULTICHANNEL SEISMIC DATA

By M.W. Lee, W.F. Agena, and D.R. Hutchinson

### ABSTRACT

In September 1986, 1,370 km of deep crustal reflection profiles were acquired in the Great Lakes region as part of the Great Lakes International Multidisciplinary Program on Crust Evolution (GLIMPCE). The energy source was a 127.5 L (7,780 in.<sup>3</sup>) tuned airgun array, and 20 seconds of data were recorded at each shot point. Preliminary stacked sections were dominated by the coherent multiple and side-scatter noise. Post-stack dip filtering suppressed strong side-scatter noise of low apparent velocity but it did not enhance the subsurface reflections as desired. Predictive deconvolution suppressed the short-period reverberations caused by source and receiver ghosts but it could not adequately handle the long-period (on the order of 400 ms) multiples. These strong coherent noises combine to not only mask shallow subsurface reflections, but also make it extremely difficult to analyze weak reflections from the lower crust and upper mantle. To perform a geologically sound interpretation and to properly migrate deep reflections, pre-stack processing techniques based on the moveout differences between signal and noise are required. Therefore, dip filtering in the shot domain was applied in order to suppress the side-scattering noise, and time-variant dip filtering in the CDP (common depth point) domain was performed in order to reduce the water-bottom multiple interference.

These pre-stack processing techniques were highly successful in reducing the coherent noise in the GLIMPCE seismic data. A post-stack, signal-enhancement technique based on the strength of the reflected energy significantly improved the visual quality of the reflection profiles, enabling original data, rather than line-drawing interpretations, to be used in presenting small-scale illustrations.

### INTRODUCTION

Multichannel seismic data over the Great Lakes (fig. 1) were acquired by Geophoto Services, Ltd., a Canadian subsidiary of Geophysical Service Inc. (GSI), for the U.S. Geological Survey (USGS) and the Geological Survey of Canada (GSC) as part of the Great Lakes International Multidisciplinary Program of Crustal Evolution (GLIMPCE). 1,370 km of seismic profiles [5 profiles in Lake Superior (655 km), 1 in Lake Michigan (284 km), and 2 in Lake Huron (431 km)] with a recording length of 20 seconds were collected in order to better understand the deep structure and tectonics of the Midcontinent rift system (MRS) and the Grenville tectonic province. Additional wide-angle reflection and large-offset refraction data were recorded during acquisition of the multichannel seismic data (Hutchinson and others, 1988). This paper focuses on the details of the GLIMPCE multichannel seismic data processing done by the USGS, and all of the stacked reflection profiles are included in Agena and others (1988). Additional processing (e.g., migration) has been carried out by GSC (Milkereit and others, 1988) and is not discussed here.

The data processing was carried out in two phases (phase 1A and phase 1B). Conventional marine seismic data processing techniques were used in phase 1A in order to provide preliminary seismic stacked sections soon after data acquisition. Results of the preliminary interpretations could be fully utilized in the second phase of data processing.

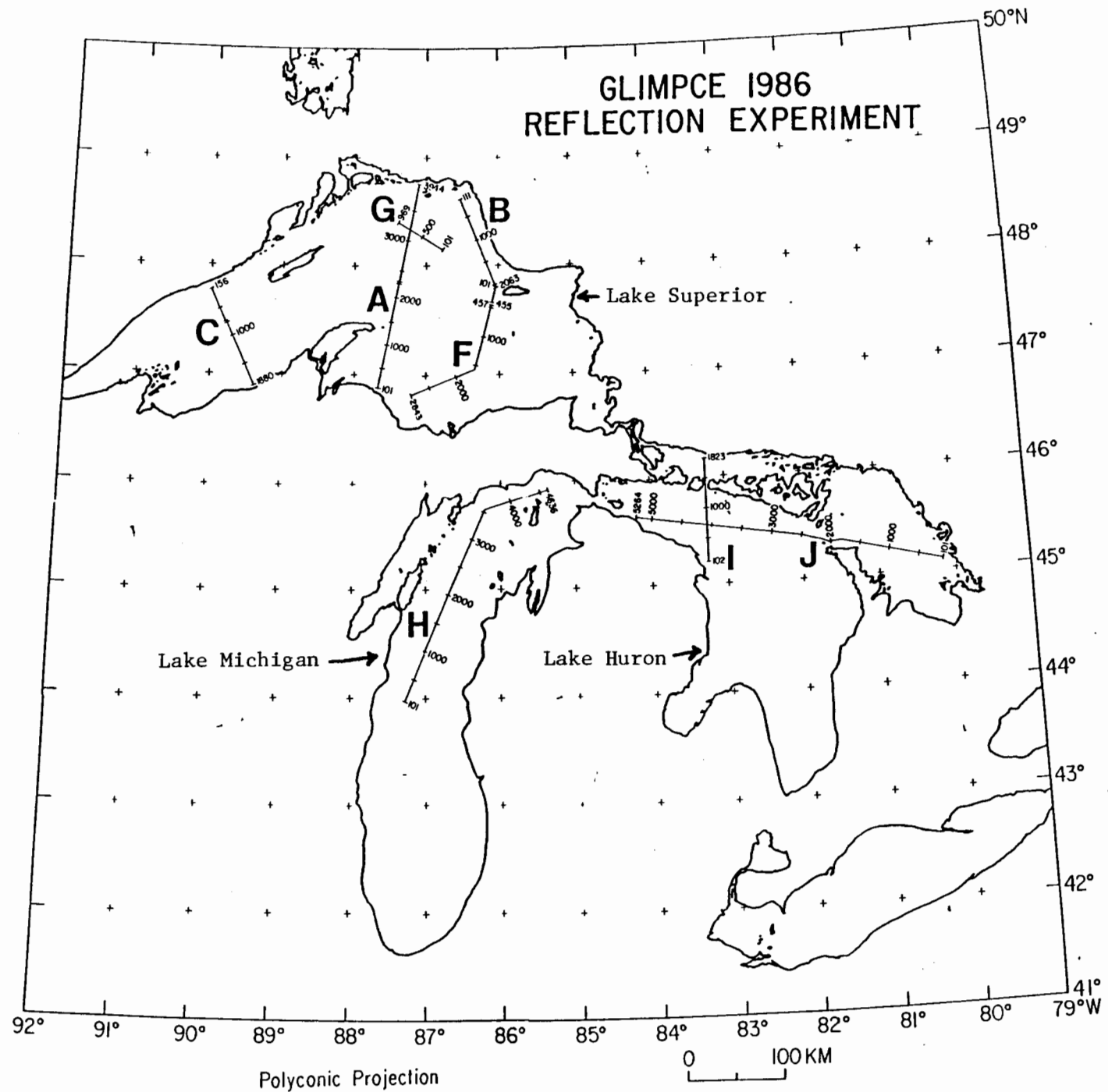


Figure 1.--Location of seismic reflection lines in Lakes Superior, Huron, and Michigan, from the 1986 GLIMPCE survey. Shotpoint locations are numbered along lines.

Preliminary processing results indicated that the seismic profiles were severely contaminated by strong water-bottom multiples for the upper part of the sections (mostly less than 5 seconds) and side-scattering noise characterized by low apparent velocity linear arrivals throughout the stacked section. These kinds of coherent noise are typical for seismic data acquired over shallow water with rough bathymetry and high-velocity rocks at or near the water bottom (Hutchinson and Lee, 1988).

In order to perform detailed geological interpretation and to better understand deep crustal reflections, it was necessary to develop some method of suppressing the coherent noise. Thus, phase 1B processing focused on the suppression of the coherent noise by pre-stack, multichannel, dip-filtering techniques based on the moveout difference between signal and coherent noise. Also, special post-stack processing techniques were developed to visually enhance the data for ease of interpretation.

The preliminary results of phase 1A processing were given by Behrendt and others (1986), and the geological interpretation based on phase 1B processing for the Keweenaw rift basin was shown in Behrendt and others (1988a).

This paper covers both the technical and operational aspects of seismic data processing. The operational aspect of the processing of GLIMPCE seismic data is important because this processing optimized available computer and human resources in a very effective way resulting in an excellent case history for the handling of large amounts of deep crustal seismic data.

#### ACKNOWLEDGMENTS

Our sincere appreciation is extended to all of the GLIMPCE members, who encouraged us throughout this project, and in particular, to William Cannon and John Behrendt of the U.S.G.S. and Alan Green of the Geological Survey of Canada (G.S.C.). Discussions with B. Milkereit and C. Spencer of the G.S.C. during the initial phase of processing proved to be very fruitful. We would also like to thank R.A. Wise for his help during the first phase of processing and the Geophysics Group members of the Branch of Petroleum Geology of the U.S.G.S. in Denver for their cooperation and expertise in helping us successfully complete this project. We thank John Behrendt and John Grow for reviewing this manuscript.

All data were processed on a VAX 11/780 computer using Digicon's DISCO seismic data processing software with additional programs developed by M.W. Lee of the U.S. Geological Survey.

#### DATA ACQUISITION

The GLIMPCE multichannel reflection data were acquired in September 1986 by Geophysical Service Inc. 1,370 km of seismic data at Lakes Superior, Michigan, and Huron were collected (fig. 1). The streamer, which consisted of 120 channels spaced 25 m apart for a total length of 3,000 m, was towed at an average depth of 10-11 m in Lake Superior and 8-10 m in Lake Michigan and Lake Huron. The seismic source used for this experiment consisted of an array of 60 airguns with a total gun volume of 127.5 L (7,780 in.<sup>3</sup>); tow depth of the source array was about 12 m in Lake Superior and 6 m in Lakes Michigan and Huron. Shot intervals varied from 50-62.5 m resulting in 30- and 24-fold data, respectively. The details of fold coverage and length of seismic lines are shown in table 1.

Table 1.--Summary of GLIMPCE seismic lines

Lake	GSI ID	GLIMPCE ID	Shotpoints	Shot Interval (in meters)	Fold	Km
Superior	A'A Part 1	A	101 - 2386	50.0	30	114.3
	A'A Part 2	A	2290 - 3944	62.5	24	103.4
	B	B	101 - 2063	50.0	30	98.2
	CC'	C	101 - 980	62.5	24	55.0
	CC' (A)	C	741 - 1880	62.5	24	71.3
	BF Link	F	101 - 456	50.0	30	17.8
	FF'	F	457 - 866	62.5	24	25.6
	FF'	F	867 - 902	50.0	30	1.8
	FF'	F	903 - 1579	62.5	24	42.3
	F'F"	F	1580 - 2089	50.0	30	25.4
	F'F"	F	2090 - 2843	62.5	24	47.1
	G	G	101 - 969	62.5	24	54.3
	Huron	1	I	101 - 1823	62.5	24
2A		J	101 - 5264	62.5	24	322.8
Michigan	3	H	101 - 4636	62.5	24	283.5
Total:			24,438			1,370.5

The data were recorded on a DFS-V recording instrument in SEG-B format with a packing density of 1,600 bits per inch. Twenty (20) seconds of data were recorded at each shot with a 4-ms sampling interval. Table 2 shows Recording parameters. A total of 625 tapes with a packing density of 1,600 bpi was collected. The survey was done by a transit satellite with intermediate fixes calculated from doppler sonar fixed and secondary verification from Loran-C. Appendix A shows additional information about data acquisition.

#### PREPARATION

In both phases of processing, we were faced with a very large data set and limited time in which to process the data. In consideration of other system users and because of the limited resources of our processing system, we were forced to implement techniques that would streamline the processing flow.

Prior to receiving the field data, preliminary tests were run to determine the best methods to streamline the processing. After analyzing the strengths and weaknesses of the computer system, we concluded that the memory (8 megabytes) and limited tape drives (8) were the major obstacles to be overcome. In order to minimize the impact on other system users, we decided that during normal working hours, only one memory-intensive process (such as demultiplexing or sorting) would be run on the computer at a time. Testing and short plots could also be run during the day. On weekends, as many processes would be run as the number of tape drives and memory available would allow. In addition, we increased the working set size of the queue from 2048 to 4096 pages in order to minimize page faults of the virtual memory of the VAX 11/780 computer. Consequently, this change also reduced the data processing time.

To further reduce the time needed for processing, we decided to make heavy use of one of the removable disk packs (360 megabytes). Within the sorting process, ten CDPs were written to disk every 4 to 5 kilometers. During the hours between 2 and 6 AM, when no computer operators were available, velocity analyses and other necessary tests were run automatically on the selected CDPs, and plots generated were usually ready for the analysts by 8 AM. This procedure enabled us to use our computer effectively 24 hours per day, 5 days per week.

#### PROCESSING PHASE 1A

Details of the processing flow for the GLIMPCE seismic data are illustrated in figure 2. Input field data were transcribed into VAX-compatible format and put into trace-sequential order. The demultiplexed shots were written to tape with a packing density of 6250 bpi (See Appendix B for details). For quality-control purposes, every 20th shot was written to disk while demultiplexing the field data. These shots were then plotted without gain to determine relative noise amplitudes. After demultiplexing the data, premature shots (misfires) were omitted from further processing. Selected bad channels (for example, channels 7 and 33 of line J) within shots were zeroed. We also decided to omit from further processing all shots containing parity errors. The number of both premature shots and shots containing parity errors was less than 2 percent of the total number of shots in the survey. Therefore, our editing did not affect the desired fold coverages.

Table 2.--Recording parameters

Instrument:	DFS V
Number of Channels:	120
Group Interval:	25 meters
Shot Interval:	(see table 1)
Fold	(see table 1)
Cable Type	120T cold
Length	3,000 meters
Format of Recorded Tapes:	SEG-B (Gapped) 276 bytes in header 314 bytes in data scan
Gain Constant:	35 db
Record Length:	20 seconds
Sampling Rate	4 milliseconds
Field Filter	Locut: 5.3 Hz with 18 db/octave slope Hicut: 64 Hz with 72 db/octave slope
Packing Density:	1,600 bpi
Record Gain Mode:	Instantaneous floating point
Total Airgun Volume:	127.5 L (7,780 cubic inches)
Depth of Airgun Array:	8-11 meters
Firing Delay:	51.2 milliseconds
Positioning:	Satellite/Sonar

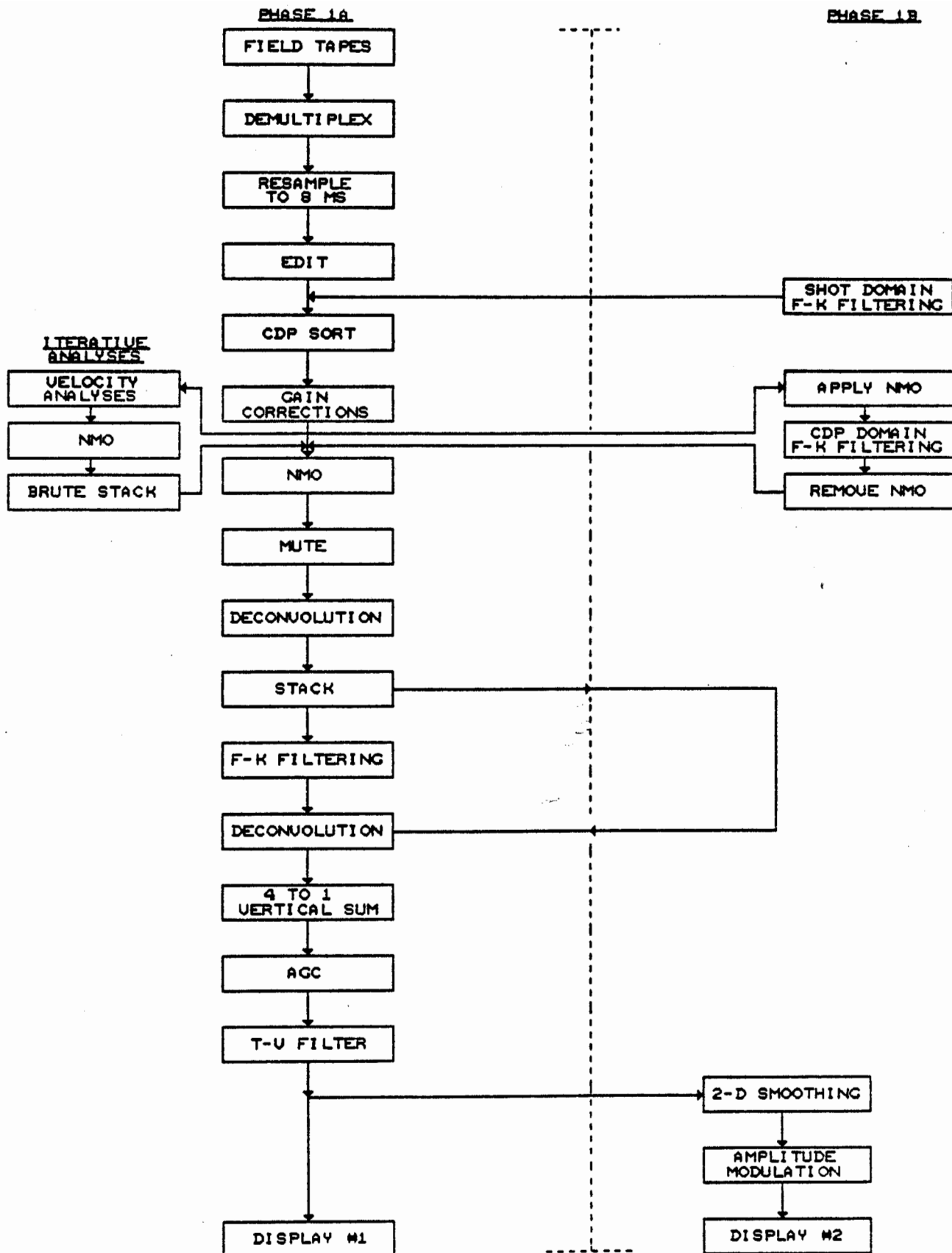


Figure 2.--Processing flow chart for GLIMPCE seismic data; left portion is phase 1A processing sequence and right portion is phase 1B processing sequence.

After analyzing the frequency content of the field data, we decided to resample the data set at 8 ms. Preliminary tests on the shot gathers showed that the dominant frequencies of the deep reflections were about 20 Hz. Because our main objective was the data processing of the deep reflections, we did not lose any relevant information by the resampling process. More detailed analyses are presented in later sections.

This resampling was done during CDP sort and effectively decreased the overall processing time by a factor of two. The data were then sorted into CDP order. During sorting, the 51-ms time delay that had been used in the recording of the data was removed and ten CDPs every 4-5 km were written to disk for quality control and analysis. In most of our analyses, we did not need to look at the complete 20 seconds of recorded data; therefore, usually 6,000 to 8,000 ms of the selected CDPs were written to disk. This process enabled us to decrease input/output time during the analyses by another factor of two.

A  $T^m$  gain analysis was performed on selected shots ( $T$ : two-way traveltime). The "m" value varied from 1.7 to 2.4 depending on the offset and noise content. In general, the near 24 traces (channels from 96 to 120) contained more noise than the far traces, making it difficult to process this data set with constant gain. Therefore, we decided to apply automatic gain control (AGC) with a 1,000-ms window after  $T^{1.7}$  gain application for the near 24 traces. The purpose of constant gain application is to eliminate the dim spots created if only AGC is applied to the data.

After sort, velocity analyses at every 4 km were performed using constant velocity stacks of 10 CDPs each. Due to the lack of detectable moveout below 5-6 seconds, all velocity analyses were performed using 8 seconds of the data. Near trace plots generated during the demultiplexing did not show any reliable reflections mostly due to the dominance of coherent noise, making it difficult to pick a reasonable velocity. In order to overcome this problem, we picked a rough velocity and applied it to every fourth CDP to produce a brute stack for the upper 6 seconds. This brute stack section provided relevant information for picking reasonable velocities, such as location of structures, problem areas, and peg-leg multiples, etc. The brute stack showed good reflections within the MRS beneath Lake Superior (Lines A-G), but disappointingly few reflections in the Precambrian crust assumed to underlie Lakes Michigan (Line H) and Huron (Lines I and J) except for the Grenville Front. Based on the brute stack section, we performed velocity analysis again. Even though this velocity-analysis scheme provided good stacking velocities between 2-6 seconds, especially in Lake Superior lines, it was still difficult to pick shallow velocities between 0-2 seconds. Thus, we relied on velocity analysis of the refracted arrivals on selected shot gathers for the shallowest part of the section.

After iterative velocity analyses, normal moveout (NMO) correction was applied; mutes were then applied in order to eliminate nonreflective energy and any NMO-stretching of the traces due to offset.

We made deconvolution tests and chose a 3-window spiking deconvolution (with 1 percent white noise added). The deconvolution operators were applied in a time- and space-variant way, and the deconvolution operator lengths were varied along the line to approximately compensate for varying water-bottom depths. The first deconvolution window (approximately 0-3 s) was chosen mainly to attack short-period reverberations owing to shot and receiver ghosts and water-bottom

multiples. The second deconvolution window (approximately 3~11 s) was chosen in order to suppress peg-leg multiples. The third window (approximately 11~20 s) was chosen in order to sharpen up the diffused wavelet from the lower crust and upper mantle.

The sequence for the deconvolution application shown in figure 2, (e.g., NMO-MUTE-DECONVOLUTION) is not the conventional processing sequence, which is MUTE-DECONVOLUTION-NMO-MUTE. The reasons for our decision to use the unconventional sequence (fig. 2) were twofold:

1) This sequence eliminates the extra mute step (and therefore, some extra processing time). Because of the limitation on the spatial interpolation of the deconvolution operator on the DISCO system, we could not apply the deconvolution operators in the desired space-variant way without mute before deconvolution. Hence, we could not use DECONVOLUTION-NMO-MUTE, which also would have eliminated an extra mute step.

2) Theoretically, this sequence does a better job of suppressing the long-period, water-bottom multiples. The water-bottom multiple period in the original CDP gather changes with propagation time due to the difference of the ray path along the water column. However, the NMO-corrected CDP gather has a consistent multiple period. Thus, predictive deconvolution worked better on the NMO-corrected CDP gather.

An example of the stacked section with a CDP interval of 12.5 m generated by the phase 1A processing sequence without post-stack processing is shown in figure 3. The low apparent velocity linear moveout events (side-scattering noise) dominate the section. This linear moveout noise persists throughout the recording time. Also, there are strong water-bottom multiples above 1 second.

In order to increase the signal-to-noise ratio and manage the stacked data in a more convenient way, we applied the following post-stack processing.

A dip-filtering (F-K) scheme was applied using 13 traces (pass band  $\pm 12$  ms/trace) to suppress the linear-moveout, side-scattering noise. This F-K processing suppressed the coherent noise somewhat, but did not enhance the reflections as desired. In order to increase the temporal resolution, we applied a post-stack deconvolution, consisting of a second-zero crossing gap deconvolution applied in a time-variant way: first window, from 0~8 seconds; and second window, from 8~20 seconds. Following deconvolution, the data were vertically stacked, which means four adjacent CDPs were summed to yield a "super-CDP" trace, effectively spaced 50 m apart. The purpose of this vertical stack was threefold: (1) to reduce the number of traces in a manageable way for plotting, migrating, and other post-stack processing; (2) to increase the signal-to-noise ratio for nearly horizontal reflections; and (3) to serve as an additional dip-filtering process for the side-scatter noise.

The effect of vertical stack can be explained as a two-dimensional filtering. Figure 4 shows amplitude response of a 4-trace vertical summing operator with respect to dimensionless parameter  $D/\lambda$ , where  $\lambda$  is the wavelength and  $D$  is the trace spacing. The highest signal moveout on the stack section is about 4 ms/trace or apparent velocity of 3,100 m/s. If we assume that dominant frequency of the signal is in the range of 25 Hz, then the  $D/\lambda$  is about 0.1. Therefore, based on figure 4, we can observe that the signal amplitude with apparent velocity of 3,100 m/s is reduced about 2-3 db due to vertical summing. However, most of the signal

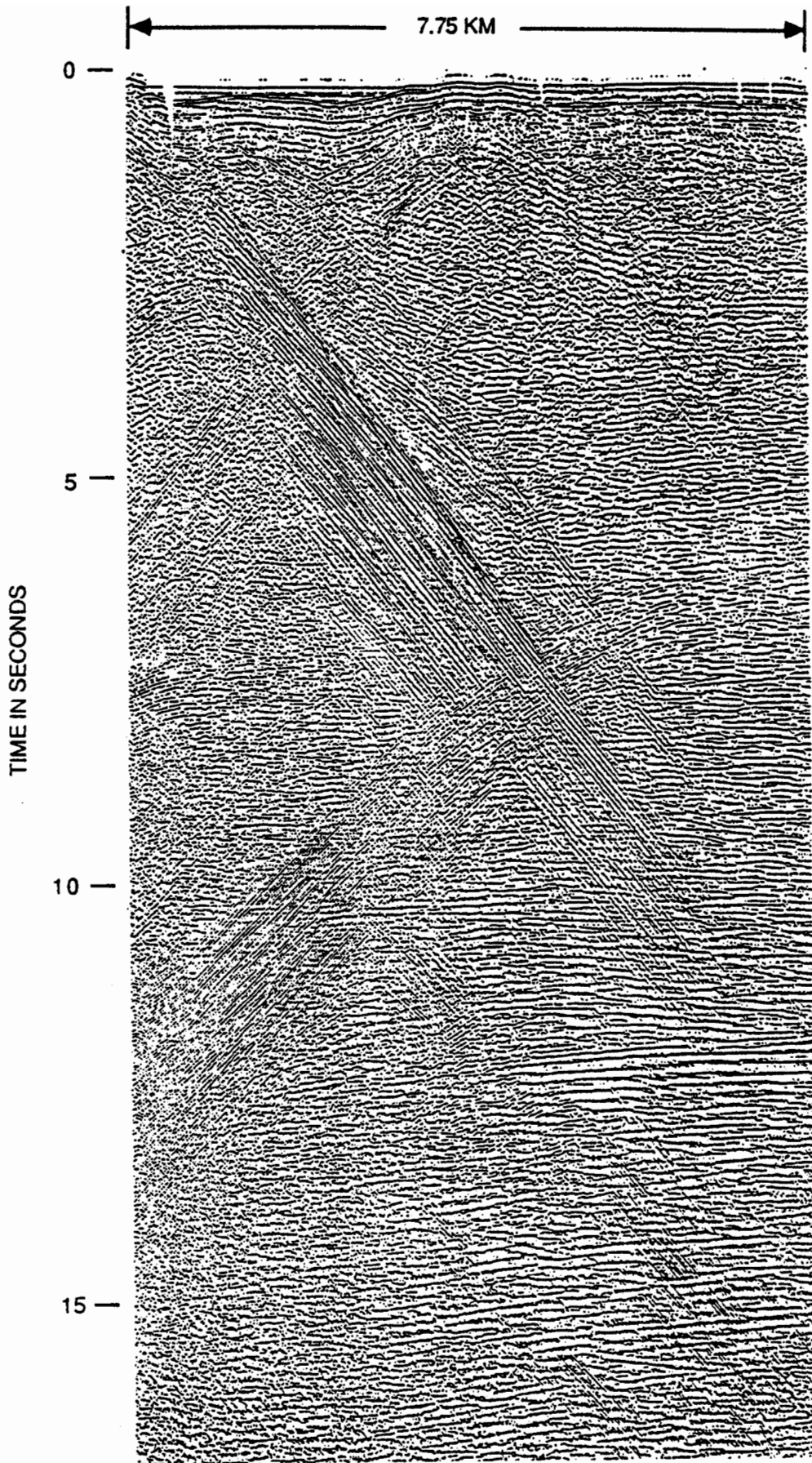


Figure 3.--Example of stacked seismic section near shot point 3300 of line A with 12.5-m CDP interval by phase 1A processing showing coherent noise problem. The same section using the second phase processing is shown in figure 12.

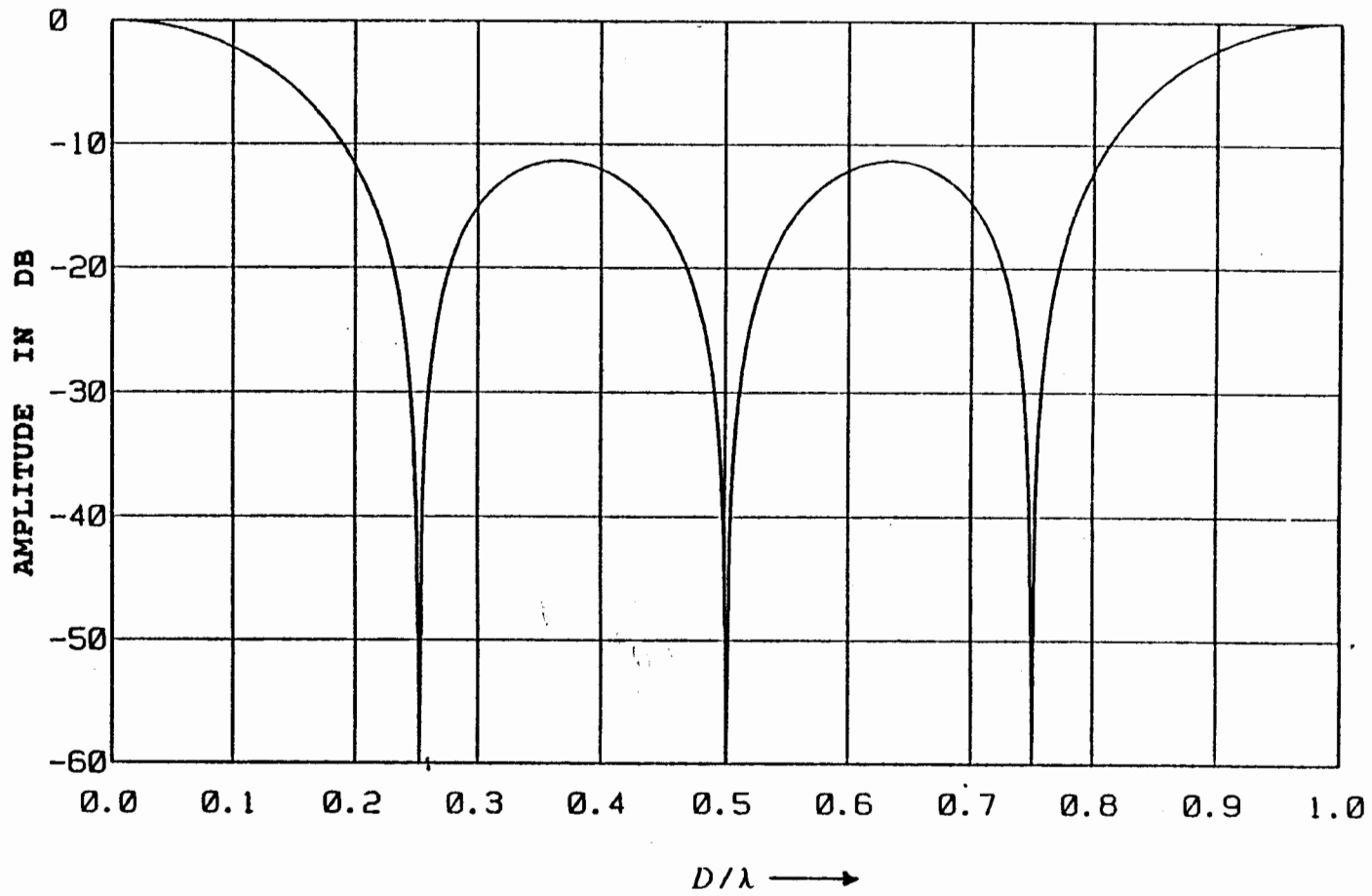


Figure 4.--Amplitude response of 4-trace vertical stack operator. D is a trace interval and  $\lambda$  is a wavelength.

has much higher apparent velocity, and amplitude reduction of the signal due to vertical summing is negligible in this data set.

The coherent side-scatter noise has a dominant moveout of about 14 ms/trace in figure 3. As mentioned previously, this noise has a broad spectrum between 10 and 45 Hz.  $D/\lambda$  for 10 Hz coherent noise is about 0.15. Therefore, side-scatter noise amplitude was reduced anywhere between 6-60 dB by vertical summing. In summary, vertical summing suppressed additional remaining coherent noise without degrading signal to the GLIMPCE seismic data. The final post-stack processing was application of 2,500 ms AGC and time-variant band-pass filter that eliminated high frequencies from the deeper data.

Figure 5 shows an example of a final stacked section by the sequence of processing phase 1A. This is a portion of line A in Lake Superior around shot point 3300.

Even though we could see some deep reflections and structures, this section is contaminated by water-bottom multiples and side-scattered noise, making it difficult to carry out any geologically sound detailed interpretations based on this seismic section.

In summary, phase 1A processing provided the following important results relevant to the detailed phase 1B processing: 1) all of the necessary parameters for single-trace processing, such as deconvolution, mute, and filter; 2) necessary stacking velocities; and 3) information about the problem areas requiring the most enhancement of signal-to-noise ratios. Based on our experiences with the first phase of processing, we focused our attention on suppressing the coherent noise in the second phase of processing.

#### ANALYSIS OF COHERENT NOISE

Two types of coherent noise are observed both in the shot domain (or shot gather) and in the stacked section; one is the side-scattering noise characterized mostly by a low apparent velocity linear-moveout, and the other is caused by water-bottom multiples.

The side-scattered noise can be divided into (1) that generated by distant out-of-plane sources and (2) that generated by shallow in-line scatters. Figure 6 shows the first type of side-scattering noise. The left portion of figure 6 shows the noise shot gather; the right portion shows the two-dimensional F-K (frequency-wave number) domain analysis for the time window (4-8 seconds). The F-K analysis of a seismogram is represented by its amplitude response in decibel (db) scale (db scale is shown in the right corner of the F-K plot), and a point in the F-K plot denotes a monochromatic plane (Lindseth, 1970). Thus a linear moveout event in the time-distance domain, like a shot domain, is represented as a linear trend in the F-K plot, and the apparent velocity can be computed in the following manner:

$$\text{apparent velocity} = \frac{\text{frequency} \times \text{trace interval}}{\text{dimensionless wave number.}}$$

For example, the apparent velocity of line OW in figure 6 is:

$$\text{apparent velocity} = \frac{30 \times 25}{0.5} = 1,500 \text{ (m/s)}$$

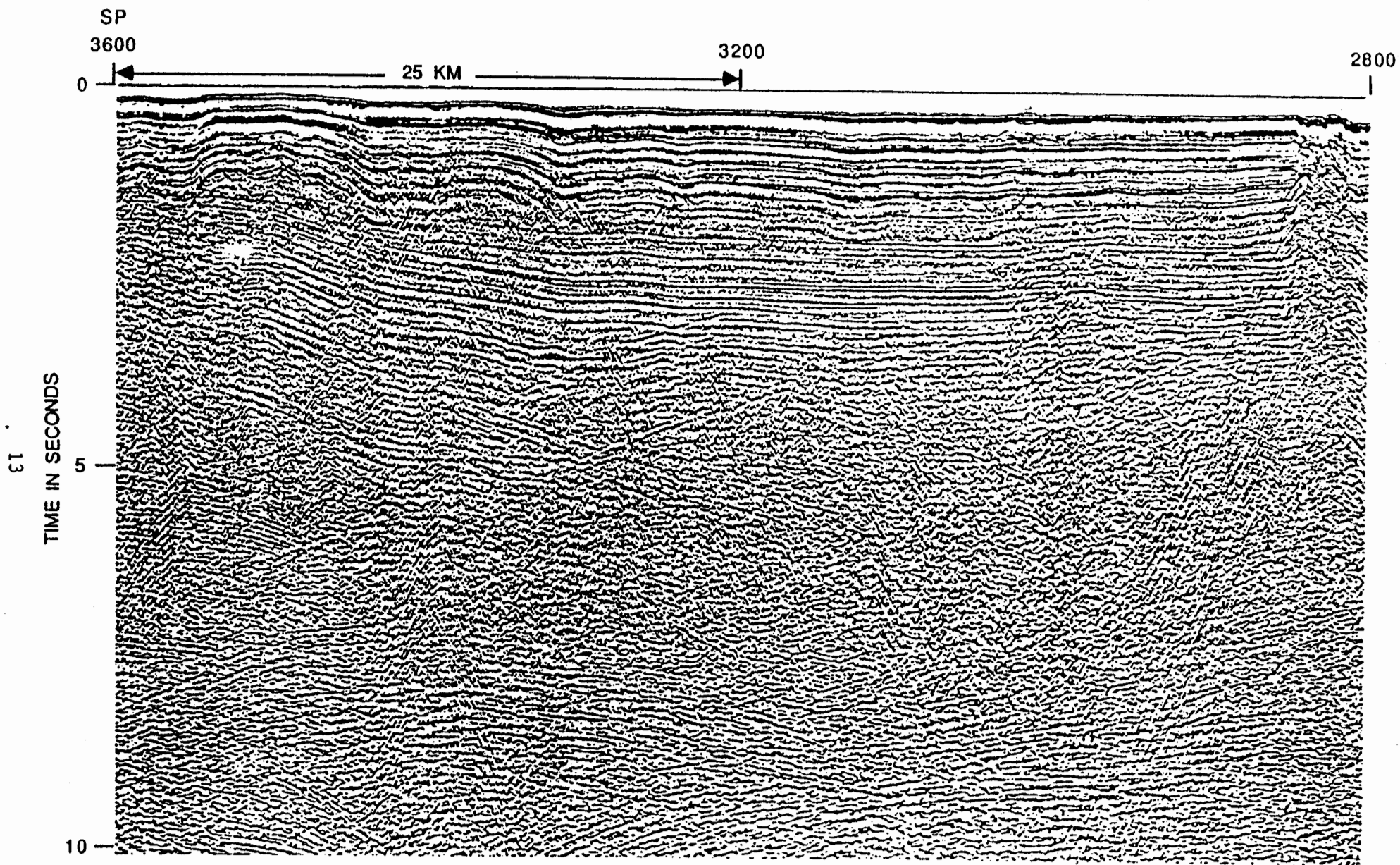


Figure 5.--Final stacked section (upper 10 seconds) with 50-m CDP interval by phase 1A processing. This is a part of line A near shot point 3300 and shows the problems associated with water-bottom multiples and side-scattering noise.

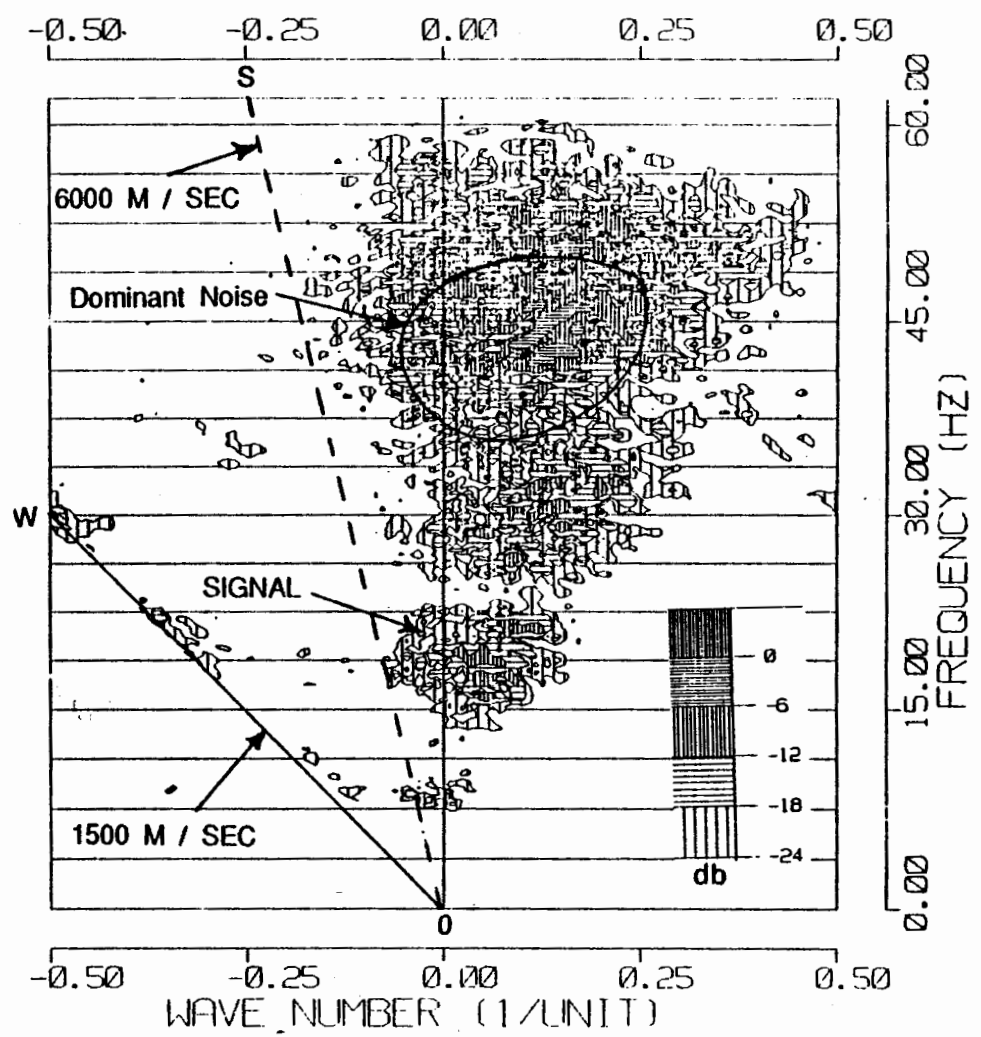
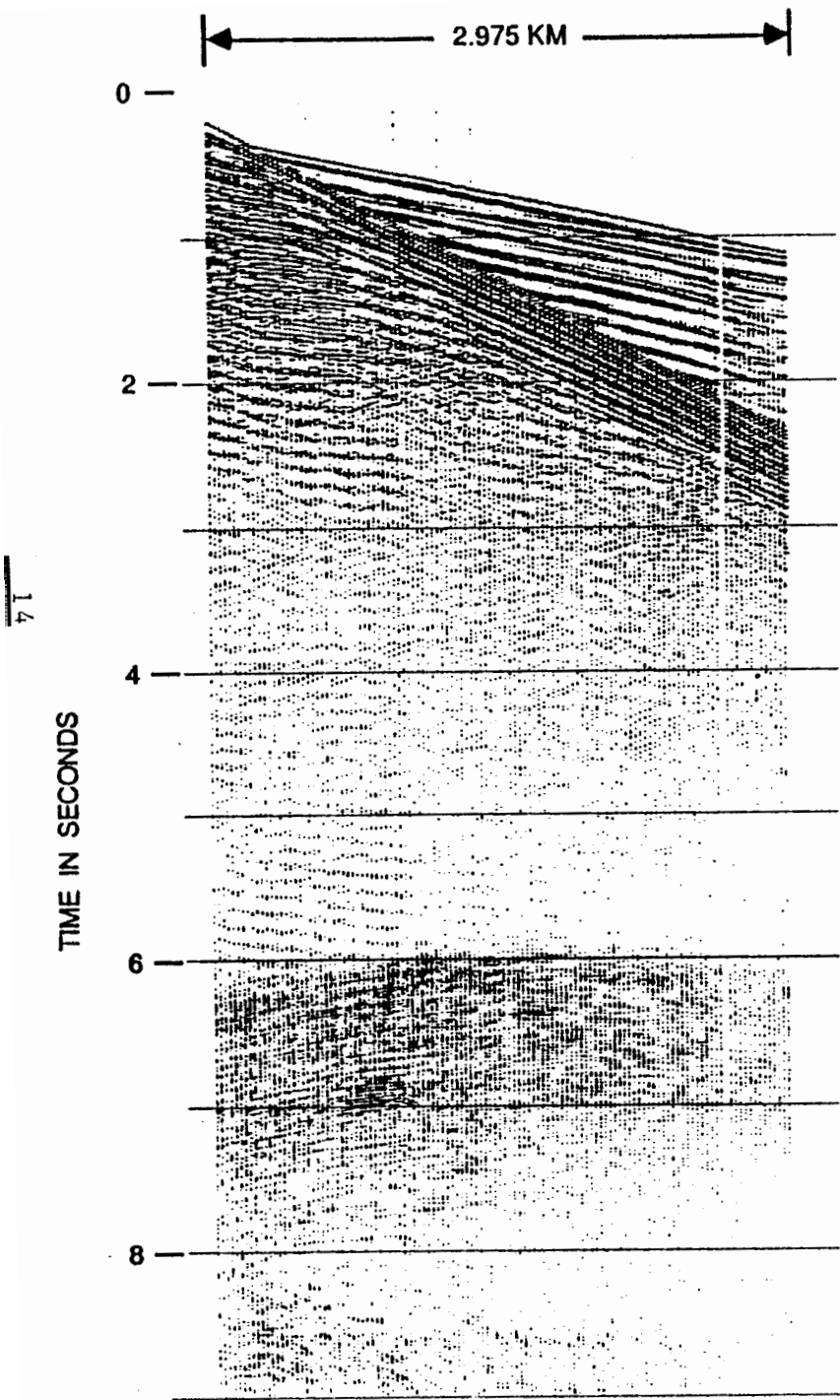


Figure 6.--Out-of-plane side-scattering noise (left) and its F-K analysis (right). Time window for the F-K analysis is 4-8 seconds, and its amplitude is plotted in db scale.

A positively-dipping event--moveout is increasing with respect to the offset distance, such as a direct arrival--is shown in the left half of the F-K plot, and a negatively-dipping event is in the right half of the F-K plot (positive wavenumber).

The arrival times of the noise around 6 seconds indicated that the noise was generated from a distant out-of-plane source. This kind of noise can be suppressed easily by utilizing the marked differences of the temporal frequency content and moveout in the CDP domain between the primaries and the noise. As shown in figure 6, the frequency content of the noise peaked around 40-50 Hz, while the dominant frequency of the primary reflections are around 10-20 Hz. Therefore, time-variant band-pass filtering is one way of suppressing this kind of noise. Also, the stacking velocities of this kind of noise are much slower than the primary event, so the stacking procedure effectively suppresses this kind of noise (Tsai, 1984).

The second kind of side-scattering noise is shown in the left portion of figure 7 and is characterized by low apparent velocity linear arrivals dipping both positively and negatively. These side-scatter noise trains are generated from shallow in-line scatters, usually on the seafloor (i.e., rough bathymetry), or near subbottom irregularities such as faults (Larner and others, 1983). Because the stacking velocity of this kind of noise is comparable to the primary reflections (Larner and others, 1983; Tsai, 1984), it is difficult to differentiate between signal and noise in the CDP domain.

Thus, this noise stacks-in coherently during normal moveout correction and stack, and appears as low apparent velocity linear events in the stacked section (fig. 3). The most effective way of eliminating the in-line scattering noise is by multichannel dip filtering (F-K filtering) in the shot gathers based on the apparent velocity difference between signal and coherent noise (Larner and others, 1985). The F-K analysis of the noise (between 4-8 seconds) shown in the right portion of figure 7 indicates that this noise has broad amplitude spectrum between 10-50 Hz and has an apparent velocity between 1,500 m/s-2,500 m/s.

A second source of coherent noise of the data was the water-bottom multiples. The lake floor of the Great Lakes area consists of a variable thickness of glacial deposits overlying Precambrian clastic, volcanic, or crystalline bedrock (Lakes Superior and Huron) and Paleozoic carbonates (Lakes Michigan and Huron).

This generally hard water bottom causes a large impedance contrast at the lake floor and generates abundant multiple reverberations. The top portion of figure 8 shows an example of a shot gather with abundant multiple reverberations; auto-correlation of the gather is shown on the bottom of the figure. As indicated, both in shot gathers and auto-correlations, approximately 24 near traces have different multiple character than the rest of the traces. The consistent trough shown around 360 ms after the peak of the auto-correlation represents the effect of the water-bottom multiple; short period ringing on the order of 50 ms for near-offset traces repressed the source and receiver ghost effects. The deconvolution operator mentioned in processing phase 1A was applied to the data shown in figure 8 and the results are shown in the top portion of figure 9 clearly indicates that the spiking deconvolution suppressed most of the short-period multiples (on the order of 50 ms), but the long-period water-bottom multiples (on the order of 300-400 ms) still remains.

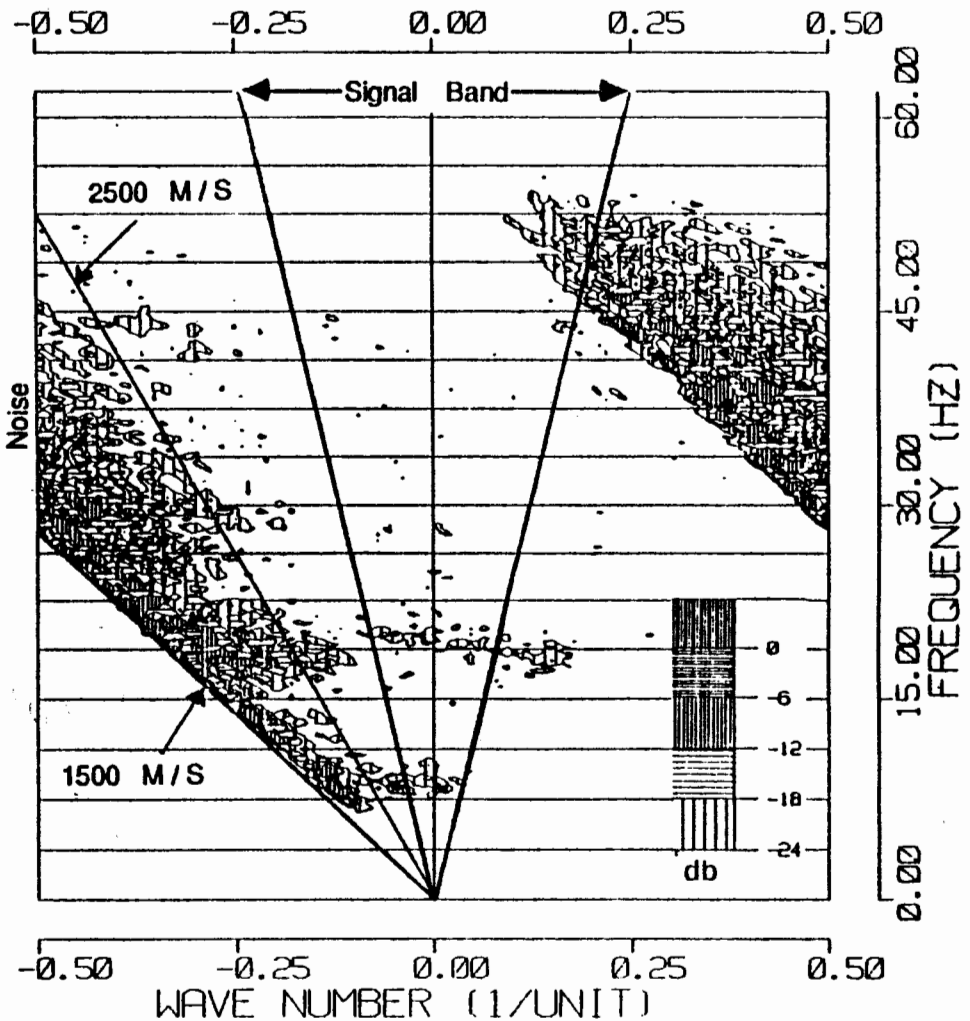
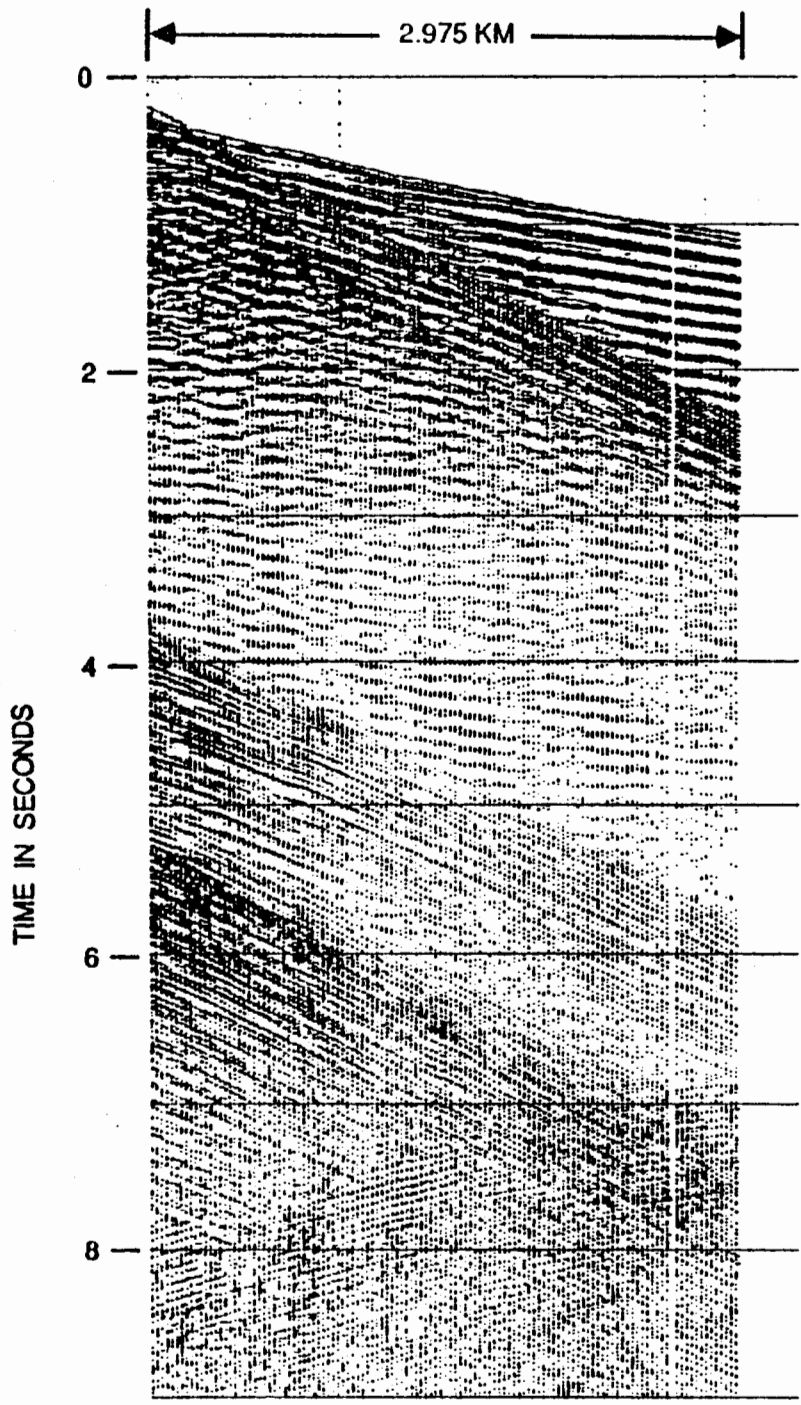


Figure 7.--In-line side-scattering noise (left) and its F-K analysis (right). Time window for the F-K analysis is 4-8 seconds, and its amplitude is plotted in the db scale.

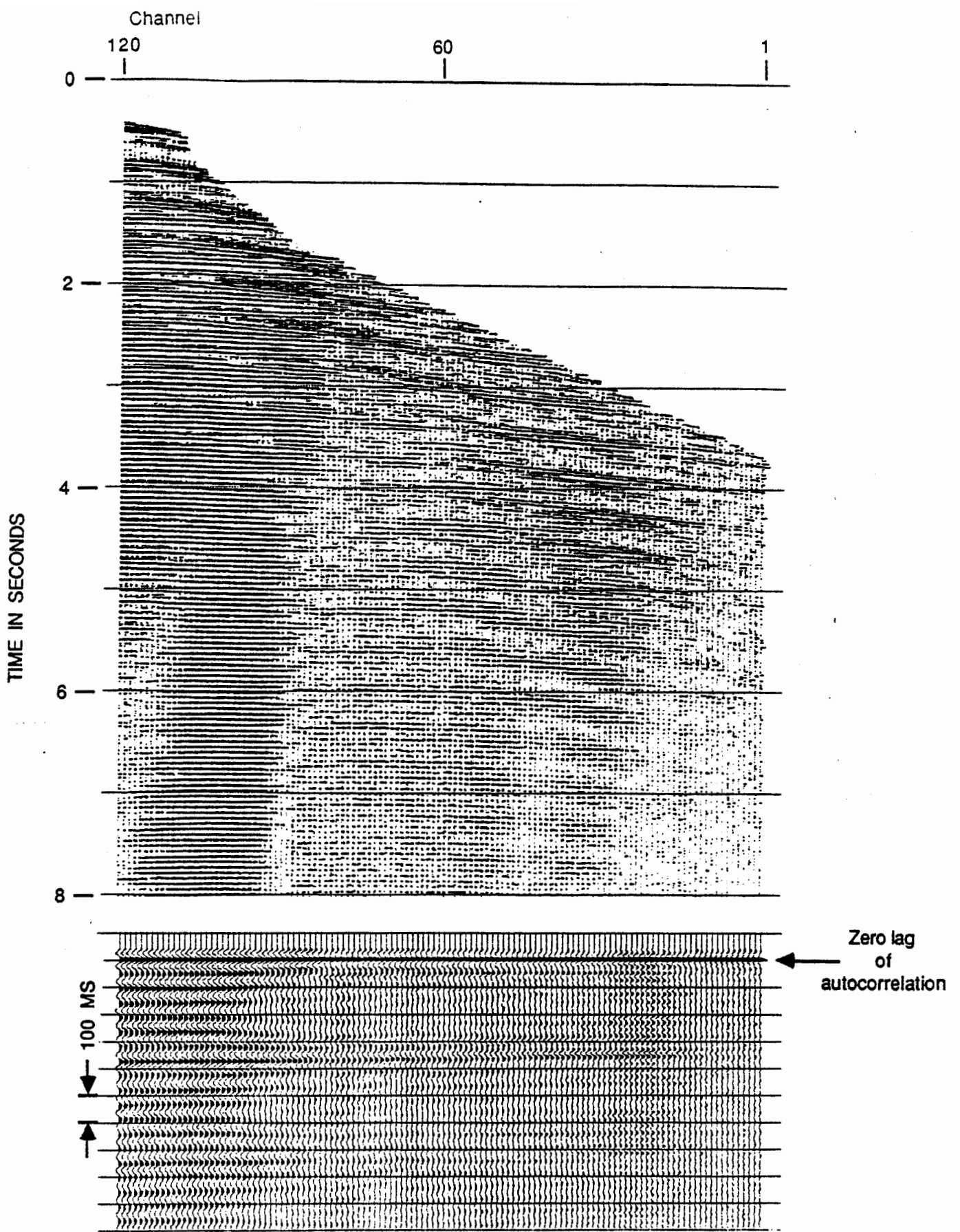


Figure 8.--Examples of shot gather showing strong multiples (top) and its autocorrelation function (bottom).

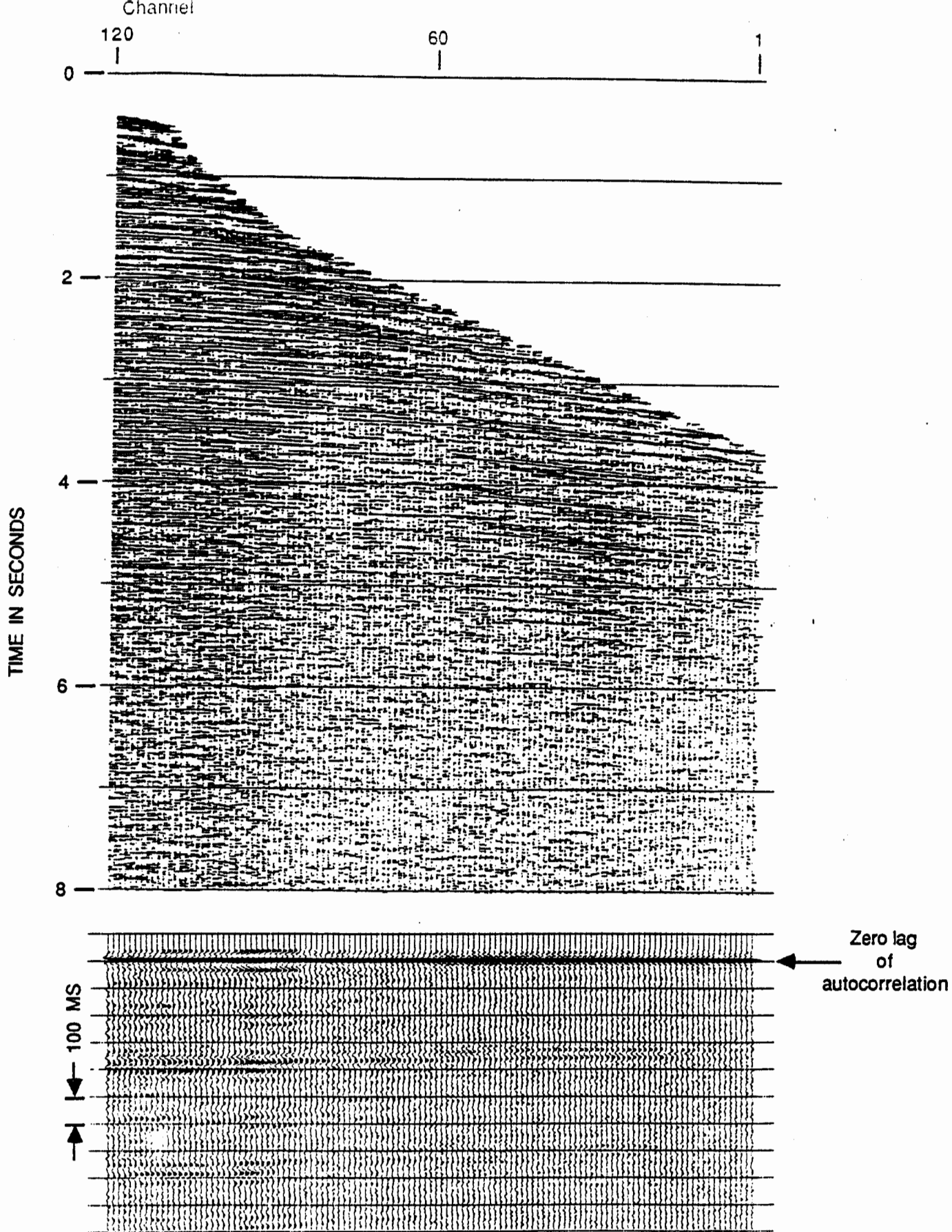


Figure 9.--Result of spiking deconvolution applied to the data set shown in figure 8 (top) and its autocorrelation function (bottom). Notice the strong trough near 400 ms after the zero-lag of the autocorrelation function.

## PROCESSING PHASE 1B

As mentioned previously, the main focus of the second phase processing was the suppression of the in-line scattering noise and water-bottom multiples. Based on the moveout analysis, velocity analysis, and F-K analysis shown in the left portion of figure 7, we concluded that the moveout of most of the seismic signal lies between +5 ms/trace to -5 ms/trace in the shot gathers. This moveout has a marked difference when compared to the moveout of the linear side-scattering noise, whose moveout varies between  $\pm 10$  ms/trace and  $\pm 17$  ms/trace.

As indicated in figure 7, linear moveout noise with a frequency content higher than about 45 Hz could be aliased back to the signal band. Therefore, the F-K filtering used 13 traces with a pass band of  $\pm 5$  ms/trace and a 4-45 Hz band-pass filtering that avoided possible aliasing energy. This 45 Hz high-cut filtering justifies the resampling to 8 ms mentioned previously. An example of dip-filtering in the shot domain is shown in figure 10. The left portion of figure 10 shows the original shot gather and the right portion of figure 10 shows the result of dip filtering in the shot domain. Notice the suppression of the low apparent velocity noise below 4 seconds on the right portion of figure 10.

As shown previously, spiking (or gapped) deconvolution technique was not optimum in reducing water-bottom multiple energy. Thus, in order to suppress water-bottom multiples, we utilized the moveout difference between primary and multiples in the CDP domain. The multiple suppression techniques used the following 3 steps.

- 1) Apply the NMO correction with a velocity function such that the primary events are over-corrected and multiples are under-corrected.
- 2) Apply dip filtering in order to reject the under-corrected event.
- 3) Remove the NMO correction applied to step 1A and proceed to the next processing step.

The basic idea behind the multiple suppression technique is very simple and similar to the decomposition of wave field by Ryu (1982). However, implementing this technique during processing required more than application of the principle. As shown in figure 5, the strong water-bottom multiples are abundant particularly for the upper 3 seconds. The water-bottom multiple strengths vary line-by-line for the GLIMPCE data, and the deepest multiple contamination is found at line H at up to 8 seconds. Therefore, the three-step multiple suppression procedure mentioned above did not have to be applied to the entire 20-second trace of the GLIMPCE data at this stage, mainly because of the time constraint. Our processing, therefore, applied this procedure to only an upper portion of the data (it varied between 3-8 s) as shown by the processing scheme in figure 11.

After gain application, the traces go through a special processing package written for this data set (GRLAKE). Briefly, the entire data trace is passed from entry point A to entry point B. The upper portion of the data is isolated and passed through the multiple-suppression processing. The data are then merged together at entry point B as described below. At entry point A, the input traces were written into a virtual memory up to 200 traces before outputting at entry point B. The upper portion of the data, for example up to 5 seconds of data, went through the LEN program, which tells the DISCO module that trace length has been changed and to process accordingly.

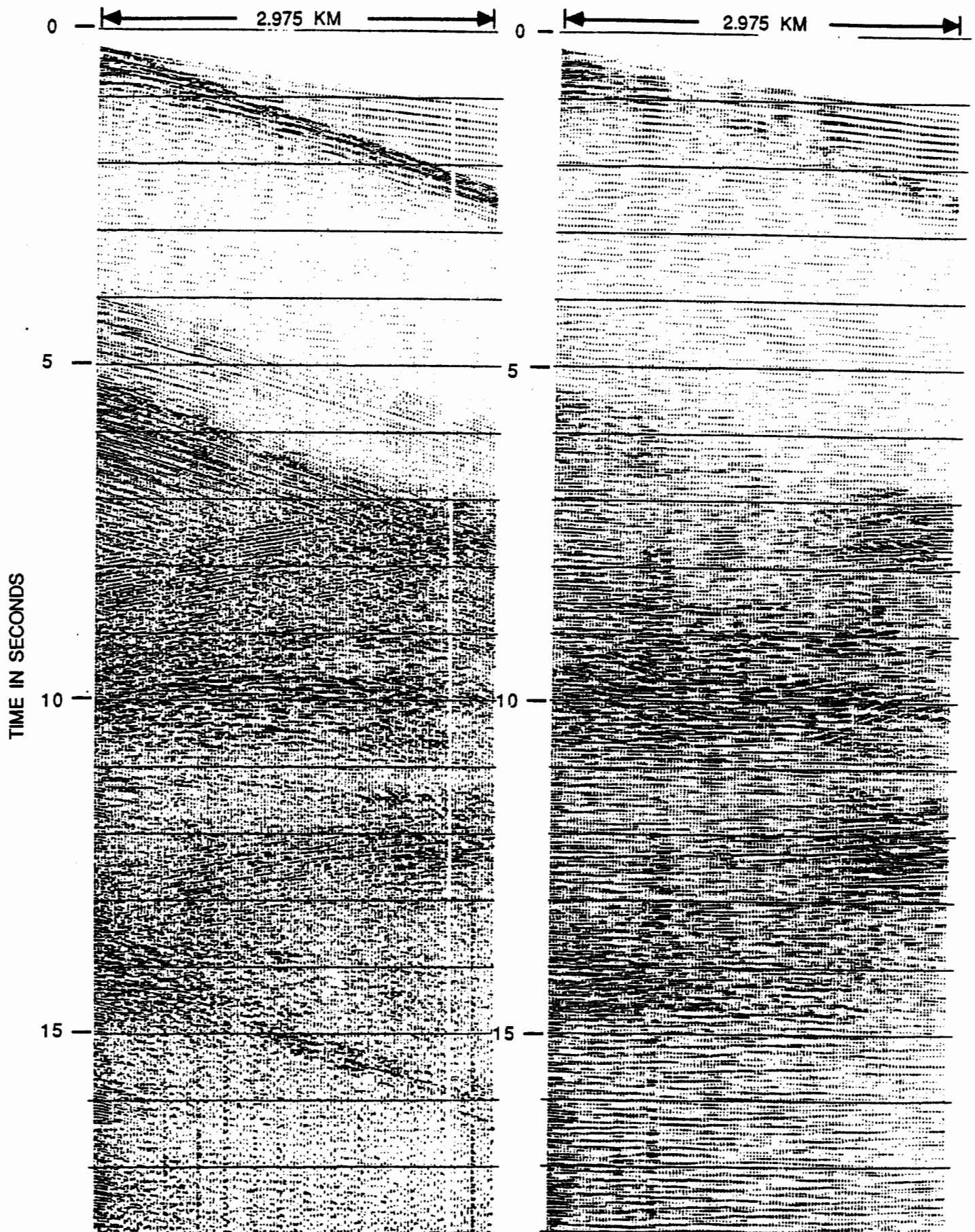


Figure 10.--Example of shot domain F-K filtering. Left: input; right: output.

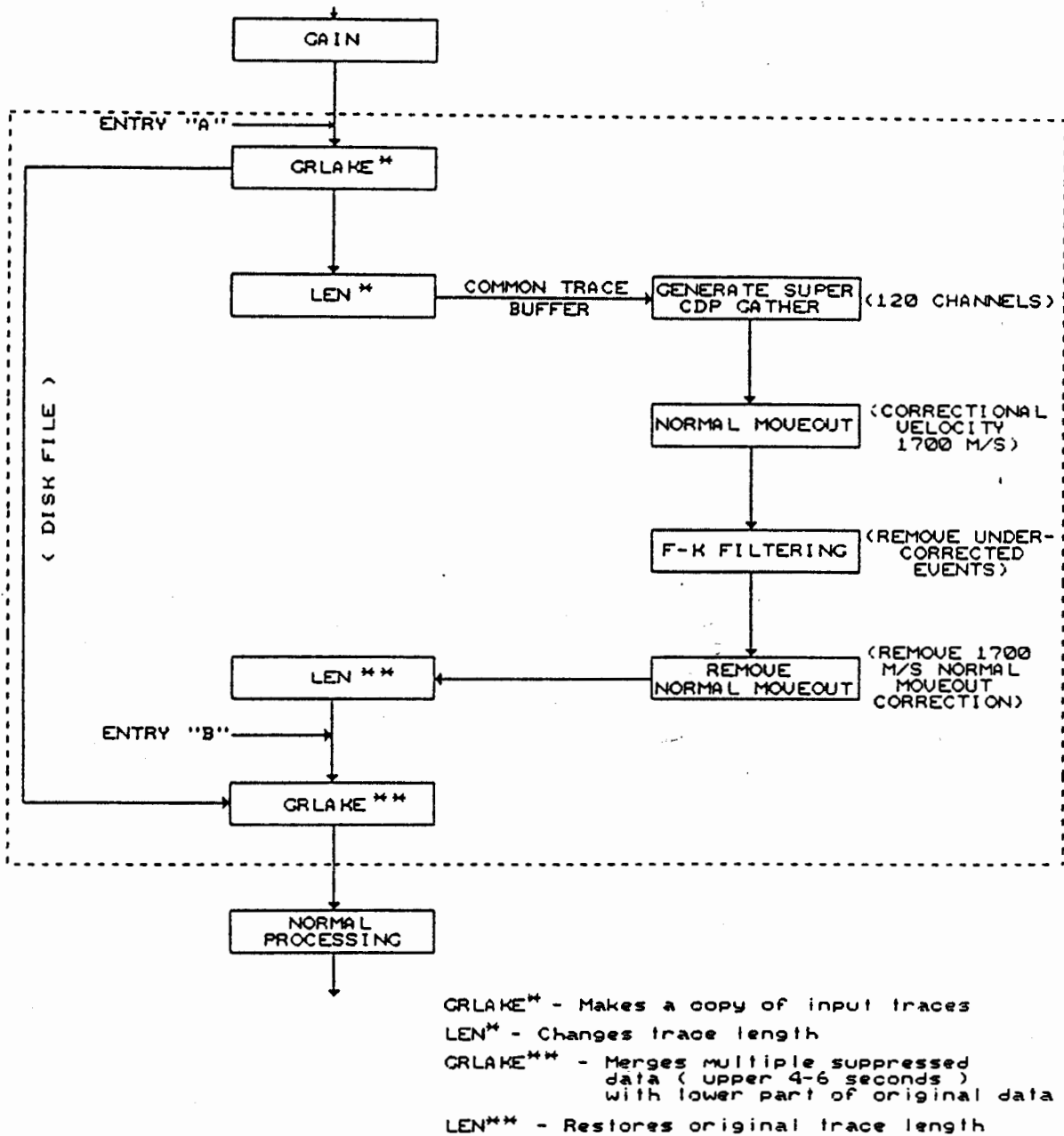


Figure 11.--Detailed computer implementation of water-bottom multiple suppression.

Before performing the three-multiple suppression steps mentioned earlier, the upper portion of the data is collected into super gathers (i.e., four or five adjacent CDPs grouped together depend on 24- or 30-fold data) prior to passing through the multiple suppression steps. The advantage of doing this super grouping is twofold; 1) reduction of the edge effect of the multichannel F-K filtering, and 2) reduction of the aliasing problem by decreasing the spatial sampling interval from 125 m or 100 m to 25 m.

After multiple suppression, the top portion of the data is merged back into the original data trace through the program GRLAKE with an overlap window in the following way:

Let  $T_i(t)$ : original input trace at entry point A  
 $T_o^Z(t)$ : output trace with multiple suppression applied  
 $t_{max}$ : length of data trace that passed through multiple suppression process  
 $\tilde{t}$ : overlap time zone.  
 $T_o(t)$ : output trace at entry point B

Then:

$$\begin{aligned} T_o(t) &= T_o^Z(t) & \text{for } 0 < t < t_{max} - \tilde{t} \\ &= \alpha T_o^Z(t) + (1-\alpha)T_i(t) & \text{for } t_{max} - t < t < t_{max} \\ &= T_i(t) & \text{for } \tilde{t} > t_{max} \end{aligned}$$

where  $\alpha$  is a linear function of time which is 1 at  $t = t_{max} - \tilde{t}$  and 0 at  $t_{max}$ . The typical overlap zone was about 1 second.

After this multiple-suppression process, the second phase processing sequence is identical to that of the first phase processing sequence up to stack as shown in figure 2.

An example showing the results of the second-phase processing technique in a region of significant side-scatter noise is shown in figure 12, which can be compared with the first phase processing of the same data shown in figure 3. Except for high-frequency side-scatter noise between 2-6 seconds, nearly all of the side-scattering noise was suppressed. Also, the strength of the water-bottom multiples has been significantly reduced. The only inferior quality of the stacked data shown in figure 12 (compared to that of figure 3) is the deterioration of the water-bottom reflection. Because the emphasis of this data processing intentionally focused on the deep reflections, this technique did not enhance shallow reflections less than 1 or 2 seconds reflection time. Time variant F-K filtering in the shot domain would probably have produced a better section for the shallow reflections.

Figure 13 shows another example of the data processed using the second phase of the processing techniques and can be directly compared to that shown in figure 5. Notice the remarkable enhancement of the signal-to-coherent-noise ratio for all 10 s of the data shown in figure 13. The quality of this figure justifies the extensive, pre-stack processing techniques described in this article.

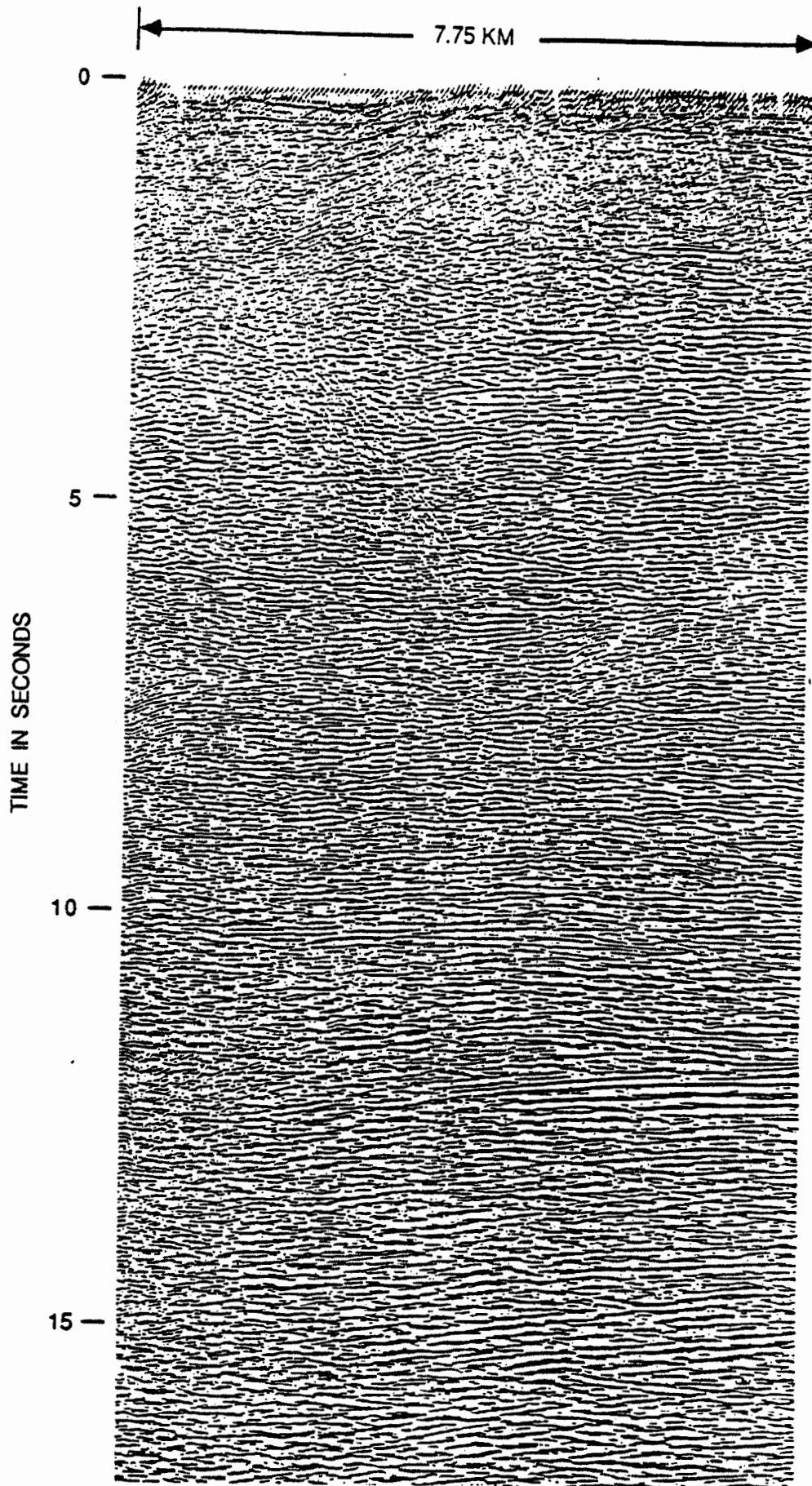


Figure 12.--Example of stacked section near shot point 3300 of line A with 12.5-m CDP interval by phase 1B processing. Compare with figure 3 to see the effect of pre-stack processing in suppressing coherent noise.

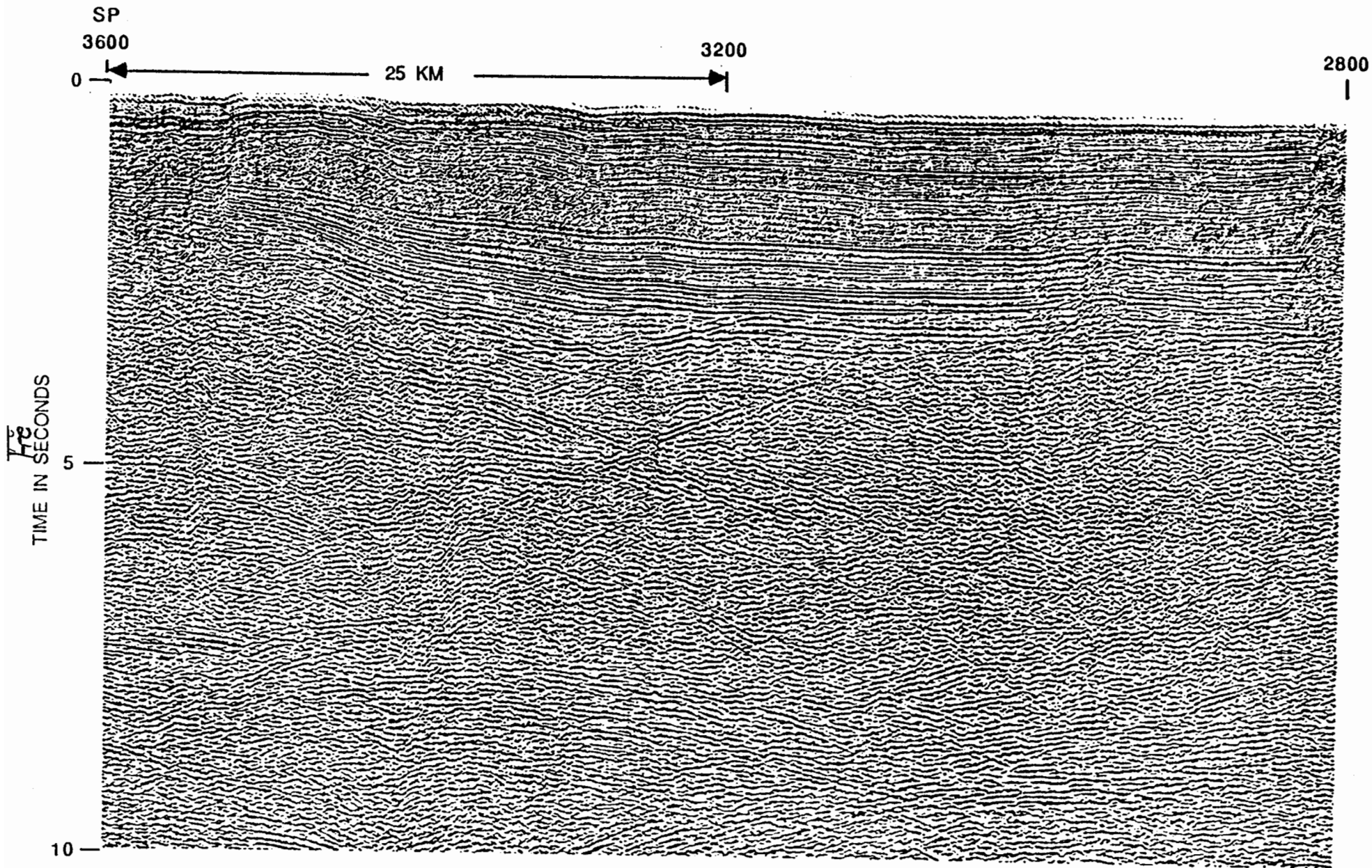


Figure 13.--Final stacked section (upper 10 seconds) with 50-m CDP interval by phase 1B processing is compared to figure 5 for the clarity of the reflection profile and significant signal enhancement. This is a part of line A near shot point 3300.

### POST-STACK PROCESSING TECHNIQUES

Even though the second-phase processing produced a significantly improved seismic section, the data were still not clearly displayed at the small scales typically used in publications. In order to enhance the visual appearance of the seismic sections and to be able to use the seismic data rather than line-drawing interpretations for visual display, we developed two techniques applied post-stack: a two-dimensional smoothing filter and amplitude modulation.

The two-dimensional smoothing filter is defined as:

$$\tilde{T}_{ij} = T_{ij} + \frac{\beta}{(2N+1)(2M+1)} \sum_{n=-N}^N \sum_{m=-M}^M T_{i-n, j-m} \quad (1)$$

where

$T_{ij}$  is an amplitude of the  $j$ -th time sample of the  $i$ -th trace,

$\tilde{T}_{ij}$  is output, and

$\beta$  is a scalar constant. This two-dimensional smoothing operator is a modification of a two-dimensional box filter described by McDonnell (1981). By varying  $\beta$ , we can enhance different aspects of seismic data. For example, if  $N=M=1$  and  $\beta=-1$ , then it is a Laplacian filter with a negative sign, which approximates an unvariated second-derivative operation. When  $\beta=-9/10$  with  $N=M=1$ , then this operation makes an image that looks sharper and noisier as mentioned by Benjamin (1987). When  $\beta$  is positive, the effect is to smooth the input data. We typically choose  $\beta=0.5$ .

For the final film plots for the GLIMPCE seismic data (25 traces/inch), we used  $\beta=0.5$  with  $N=M=1$ . Two-dimensional median filtering can also be used to remove spot noise (Benjamin, 1987). The effect of two-dimensional median filtering applied to the seismic section is the reduction of background uncorrelated noise or removal of isolated spikes. Reduction of the background noise or spike is important in plotting many traces per inch (e.g., 100 traces per inch) or migrating seismic data.

The amplitude modulation is defined as:

$$\tilde{T}_{ij} = T_{ij} [(T_{ij})^2 + (T_{ij}^H)^2]^{\alpha/2} \quad (2)$$

where  $T_{ij}^H$  is the Hilbert transform of  $T_{ij}$ . Depending on  $\alpha$ , we can either enhance large amplitude events or equalize the whole section.

Figure 14 shows the same area as figure 13, except with the application of post-stack processing techniques by the median filter with  $L=1$  and  $M=1$ , followed by  $\alpha=1.2$  in equation (2). Most of the significant structures and reflections are visually enhanced in figure 14.

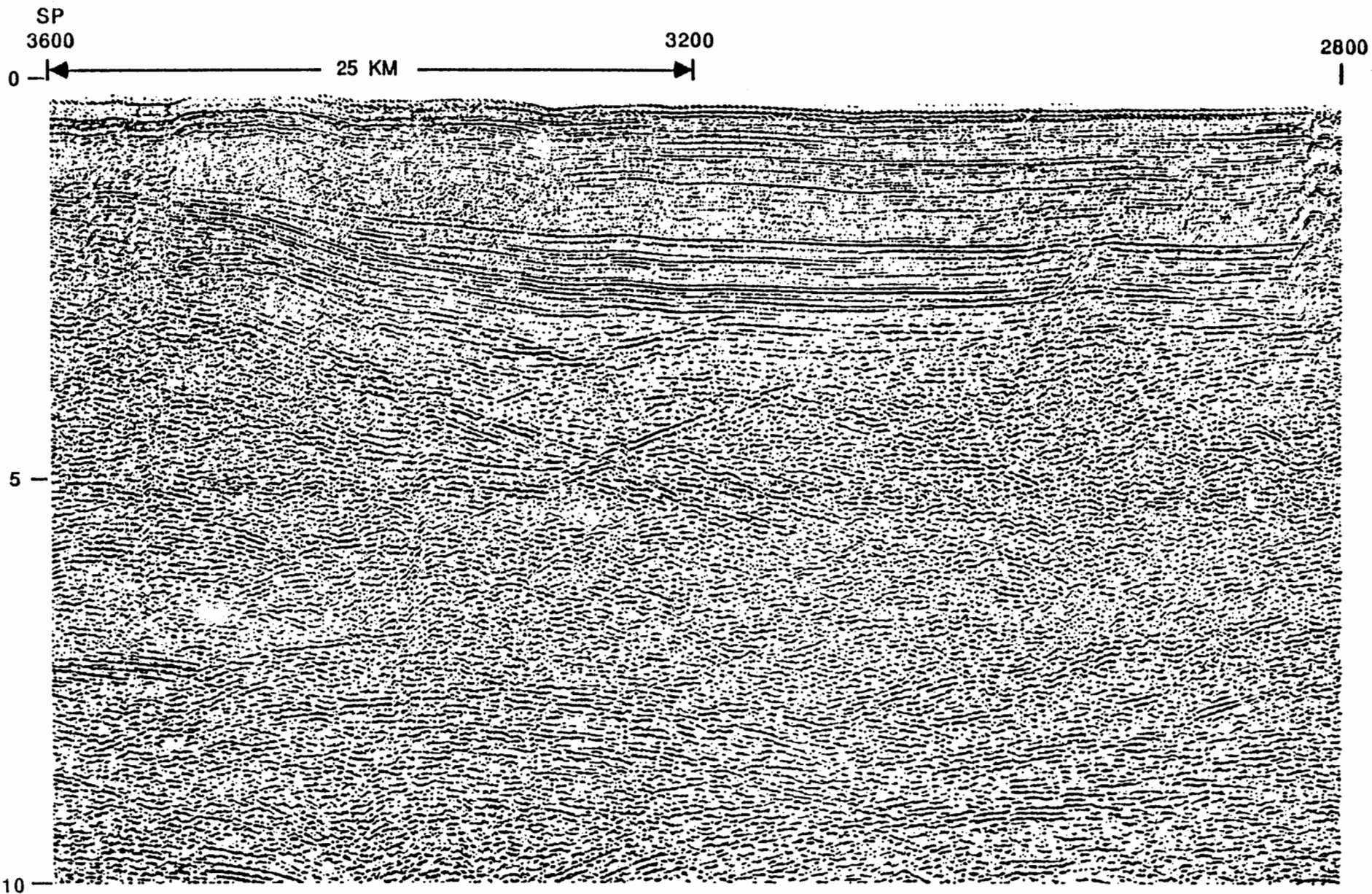


Figure 14.--The result of post-stack amplitude enhancement processing applied to figure 13. Notice the remarkable clarity of the reflections in figure 14. This is a part of line A near shot point 3300.

## RESULTS AND DISCUSSION

The second-phase processing techniques described above effectively suppressed water-bottom multiples for the upper part of the section side-scattering energy throughout the section. An example of the final stack section including post-stack signal enhancement techniques for line A ( $\approx 220$  km) is shown in figure 15. Reliable strong reflections occur within the entire profile. The axis of the Keweenawan rift basin occurs near shot point 1,500 and numerous strong events can be seen at 12-18 s (M in fig. 15). Geological interpretation and tectonic implications are given in Behrendt and others (1988b).

Figures 16-18 present a detailed comparison between phase 1A and phase 1B processing in the upper, middle, and lower crust for line A, respectively. Figure 16 shows the upper section of line A near shot point 1,500; the top portion represents the final stack section by phase 1A processing, and the bottom portion represents the final stack section by phase 1B processing. In the section using phase 1 processing, subsurface reflections above about 2 seconds are completely masked by strong water-bottom multiples, whereas side-scattering noise masks the detailed reflection configurations for the rest of the section to 5 seconds.

In contrast, the bottom of figure 16 reveals a clearly defined erosional surface near shot point 1,500 at about 1 second and north-dipping strong reflectors near 2 seconds. Also, reflections below 2 seconds are substantially enhanced. Peg-leg multiples, particularly at the left of the profile, are still present even though greatly reduced in strength. Because the differential moveout between primary and peg-leg multiples is small owing to the relative shallowness of the water bottom compared to the depth of strong reflectors, dip filtering in the CDP domain is not very effective for the entire section. Figure 17 shows similar displays for the middle portion of the section (5-10 seconds) near shot point 2,500, and figure 18 shows the bottom part of the section (10-15 seconds) near shot point 500. In each case, the second phase processing yields a superior record section with stronger, more continuous reflections that are more easily interpreted than their counterparts in phase I processing.

The above three examples clearly illustrate the effectiveness of pre-stack dip filtering in both shot and CDP domains for suppressing coherent noise in this area.

## CONCLUSIONS

1. Side-scatter noise and water-bottom multiples are the major problems in processing GLIMPCE multichannel reflection seismic data acquired over high-impedance layers with irregular bathymetry. This observation is consistent with the conclusion made by Hutchinson and Lee (1988).
2. Conventional marine data processing, including deconvolution before and after stack, can effectively reduce short-period reverberations caused by shot and receiver ghosts. However, it could not adequately handle long-period water-bottom multiples on the order of 400 ms.
3. Post-stack F-K filtering reduced the side-scatter noise somewhat, but it could not enhance the signals as desired. Optimum suppression of side-scatter noise is gained through pre-stack, shot-domain F-K filtering, even though intensive computer processing time is required.

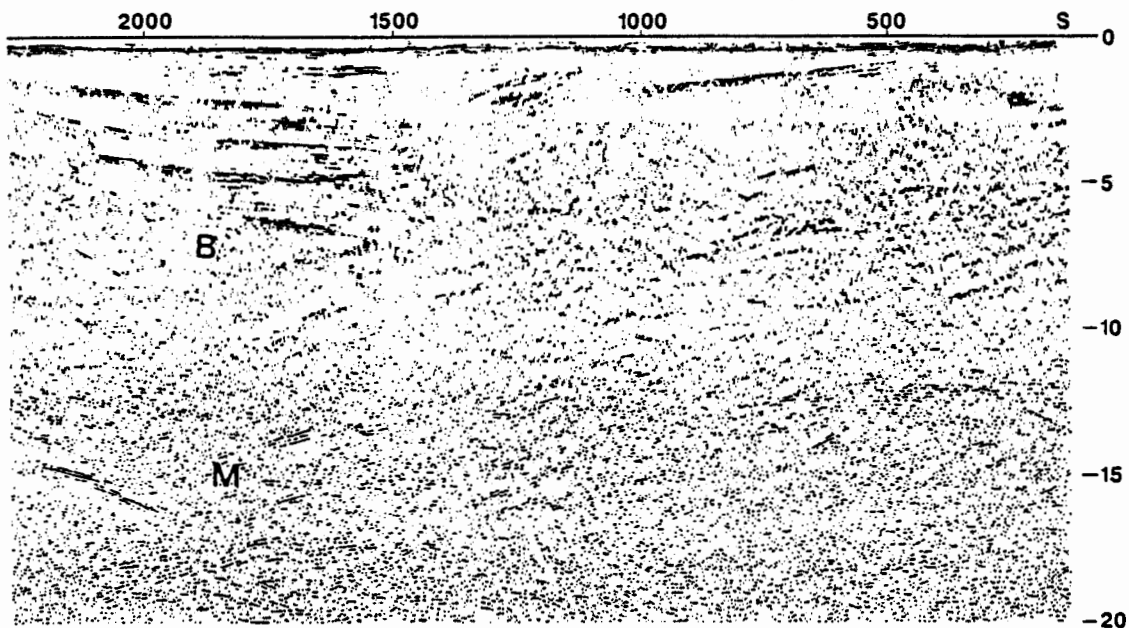
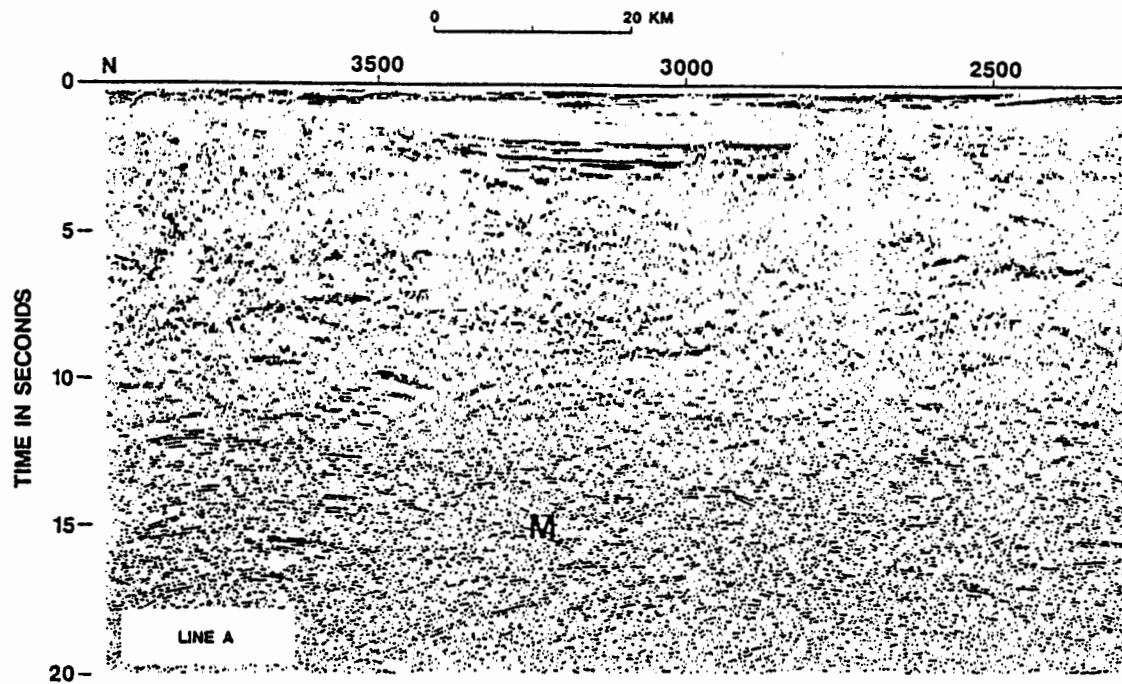


Figure 15.--Final stacked profile for line A showing Moho (M) and Archean or early Proterozoic basement (B). Total length of the profile is about 250 km and without the post-stack signal-enhancement technique, it would be very difficult to see any detailed deep reflections in this small scale.

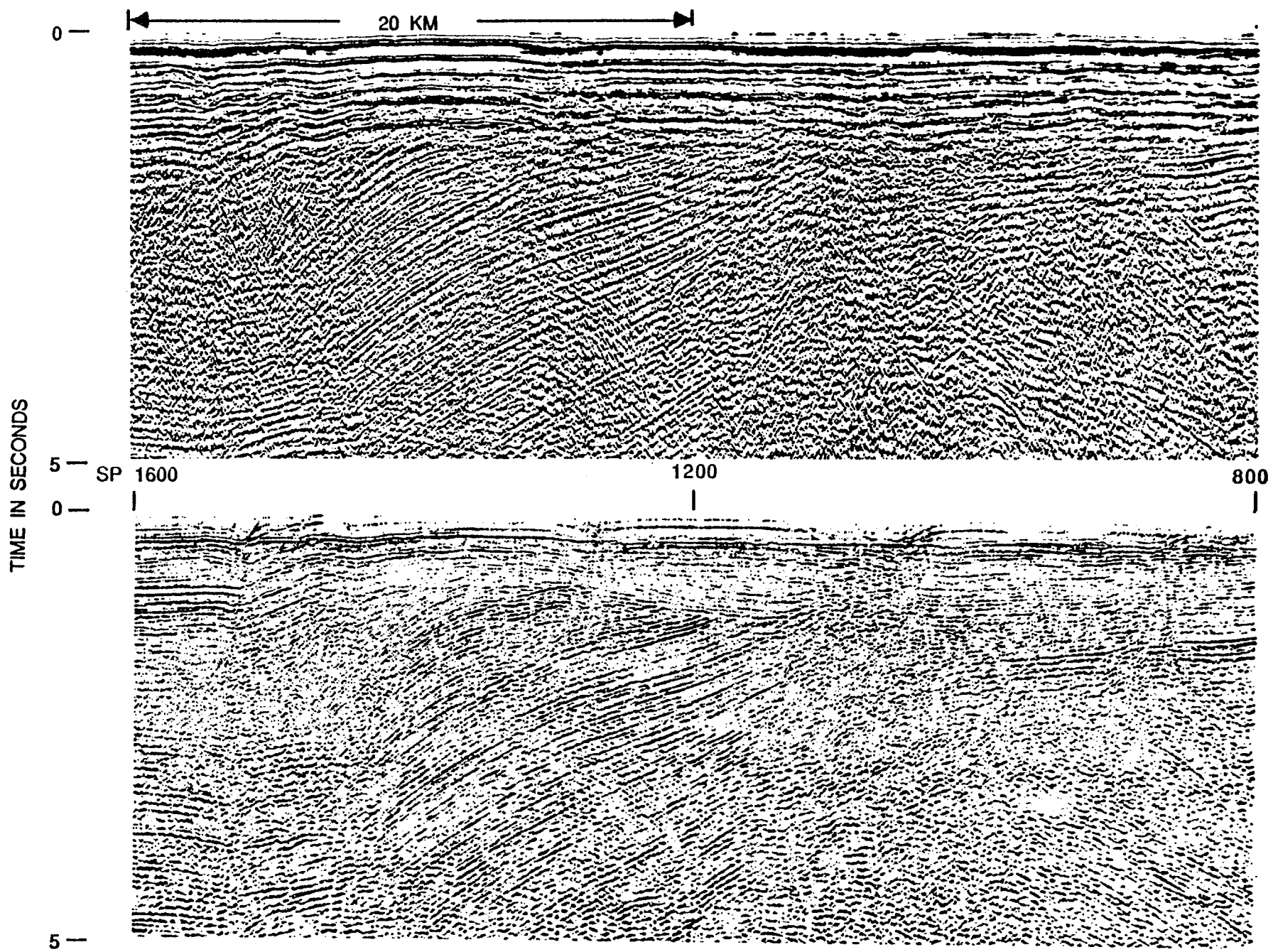


Figure 16.--Comparison between phase 1A and phase 1B data processing for the upper 0-5 seconds near shot point 1500 of line A.

bc  
69

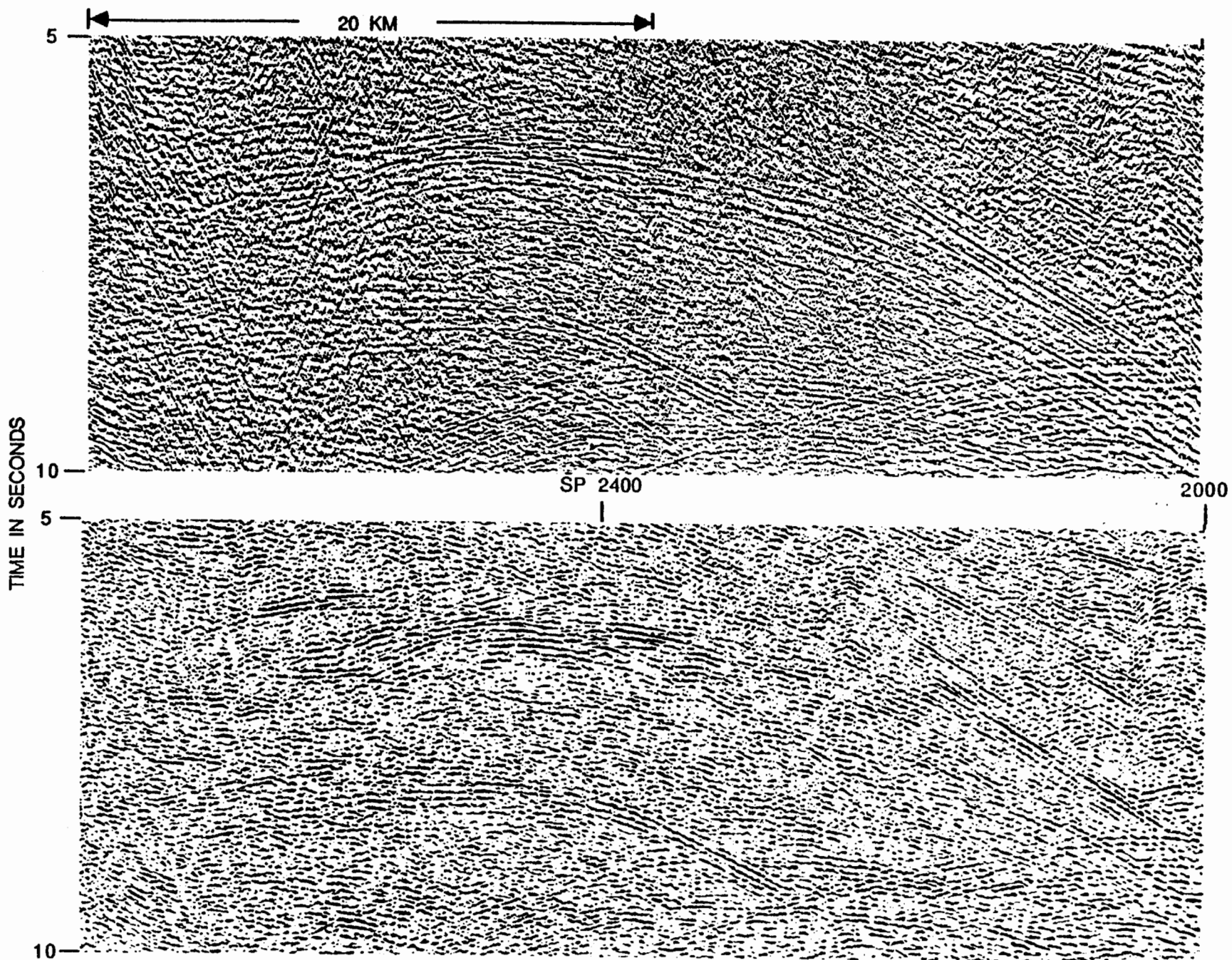
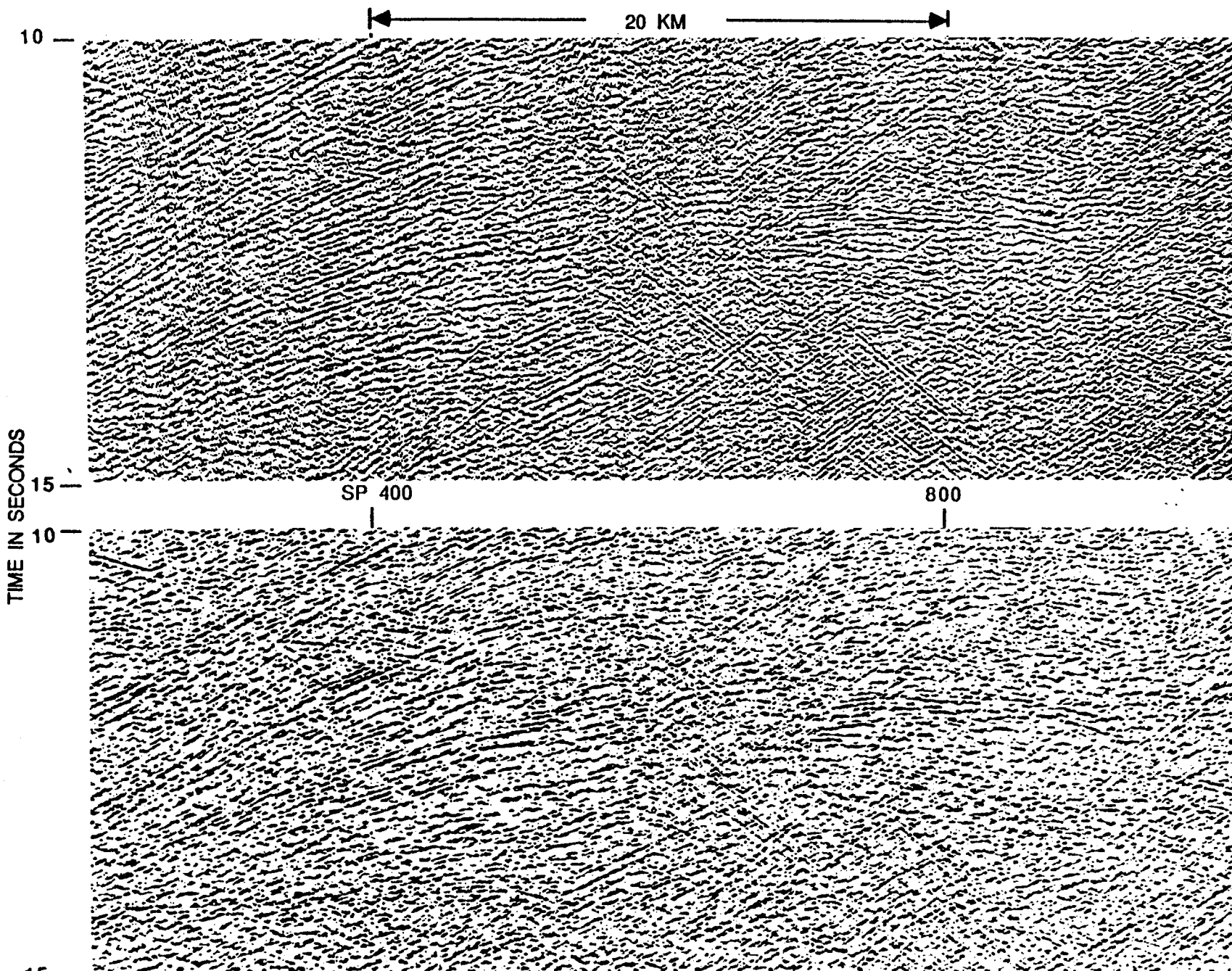


Figure 17.--Comparison between phase 1A and phase 1B data processing for the middle 5-10 seconds near shot point 2500 of line A.



15 Figure 18.--Comparison between phase 1A and phase 1B data processing for the lower 10-15 seconds near short point 500 of line A.

4. Time-varying dip filtering in the CDP domain is an effective way to suppress water-bottom multiples. However, the approach does not adequately handle peg-leg multiples.

5. Post-stack, two-dimensional smoothing and amplitude modulation techniques provide significant enhancement of reflection appearance and could replace the conventional line-drawing interpretations for deep crustal seismic data.

6. The optimization of processing sequences and computer resources, and the intermixing of existing computer programs with innovative programs were essential for the successful completion of processing 1,370 km of GLIMPCE seismic data in less than 8 months.

#### REFERENCES

- Agena, W.F., and others, 1988, 1986 GLIMPCE seismic reflection survey--stacked data: U.S. Geological Survey Open-File Report, in preparation.
- Behrendt, J.C., Green, A.G., and Cannon, W.F., 1986, Preliminary interpretation of deep seismic reflection and refraction profile across the Keweenaw Rift in Lake Superior: EOS, v. 67, no. 4, p. 1097.
- Behrendt, J.C., Green, A.G., Cannon, W.F., Hutchinson, D.R., Lee, M.W., Milkereit, B., Agena, W.F., and Spencer, C., 1988a, Results from GLIMPCE deep seismic reflection profiles over the mid-continent rift system: Geology, in press.
- Behrendt, J.C., Green, A.G., Lee, M.W., Hutchinson, D.R., Cannon, W.F., Milkereit, B., Agena, W.F., and Spencer, C., 1988b, Crustal extension on the Midcontinent rift system, American Geophysical Union, Geodynamics Series, in press.
- Benjamin, M.D., 1987, Introduction to image processing algorithms: Byte, v. 12, no. 3, p. 169-186.
- Hutchinson, D.R., and Lee, M.W., 1988, Processing and attenuation of noise in deep seismic-reflection data from the Gulf of Maine: in preparation.
- Hutchinson, D.R., and others, 1988, Description of GLIMPCE 1986 large offset seismic data from the Great Lakes: U.S. Geological Survey Open-File Report, in preparation.
- Larner, K., Chambers, R., Yang, M., Lynn, W., and Wai, W., 1983, Coherent noise in marine seismic data: Geophysics, v. 48, p. 884-886.
- Lindseth, R.O., 1970, Recent advances in digital processing of geophysical data, a review: Society of Exploration Geophysicists, p. 10.1-10.57.
- McDonnell, M.J., 1981, Box filtering technique: Computer Geophysics and Image Processing, v. 23, p. 258-272.
- Milkereit, B., and others, 1988, 1986 GLIMPCE seismic reflection survey--migrated data: Canadian Geological Survey Open-File Report, in preparation.
- Ryu, J.V., 1982, Decomposition (DECOM) approach applied to wave field analysis with seismic reflection records: Geophysics, v. 47, p. 869-883.
- Tsai, C.J., 1984, An analysis leading to the reduction of scattered noise on deep marine seismic records: Geophysics, v. 49, p. 17-26.

## APPENDIX A

This appendix contains additional information pertinent to understanding the GLIMPCE seismic data acquisition. These are edited excerpts from the Geophoto Service Ltd. report to GSC-USGS that clarify the survey with regard to the streamer and source airgun array. As can be seen from the report, many experiments were performed during the data acquisition in Lake Superior. During the survey in Lakes Michigan and Huron, the operation went smoothly and shot intervals were constant at 62.5 meters.

### SURVEY DISCUSSION

GEONAV, which utilized a Transit Magnavox satellite receiver and sonar velocities, provided the primary navigation information for this survey. For the secondary system, CAN-NAV Ltd. personnel provided Loran-C in the form of an INTERNAC LC400 Loran receiver integrated to the ONI NAVCOMP system. Geophoto operated a Texas Instruments 4100 GPS (Global Positioning System) receiver as a backup source of information.

The Geophoto 990 NAV unit provided real time navigation, while the CMS\* (Configurable Marine System) assured line control. All survey information systems were interfaced to the Texas Instruments R-980B computer of the CMS II\* integrated satellite/doppler sonar system.

The Loran-C base stations used for this survey were located at:

Sta. Dana	039 51 07.48 N	087 29 11.51 W
Sta. Seneca	041 42 50.74 N	076 49 34.50 W
Sta. Beaudette	048 36 49.65 N	094 33 16.99 W

The M/V Fred J. Agnich traveled up the St. Lawrence River and through Lakes Ontario, Erie, and Huron to reach the port of Sault Ste. Marie. Ontario at 17:00 G.M.T. on 1986 08 30. Here supplies were replenished and the vessel's crew was changed before the vessel set a course for the prospect site in Lake Superior.

At 08:00 on 08 31, the airgun array was deployed and the vessel circled to start shooting Line AA at exactly 16:00 (12:00 Eastern Daylight Time). This was a refraction data line, for which Geophoto generated shotpoints which were recorded by land-based crews and by a series of buoys which the U.S. Coast Guard had positioned in the lake. The line was shot in external start mode, with the chronometer synchronized to WWV satellite time, to provide a common time reference to the Geophoto shooting vessel and the multiple sets of recording instruments on shore. The chronometer was set up to issue the external start on every even two-minute mark. The shore stations were in a continuous record mode.

During the next three days, the crew troubleshot the streamer while working on the navigation problems. On 09 02, the satellite antenna was removed from the main mast for inspection, and reinstalled on the helideck using the GPS (Global Positioning System) cable. Port calls were made at Marathon, Ontario on 09 03 and again on 09 04 for replacement parts for the satellite unit. By 09 05, it appeared that the source of the satellite problem was that an incorrect antenna height was entered into the MX1107 RS receiver which did not accommodate the lake's elevation as compared to sea level. Geophoto's office in Calgary corrected this error while processing the navigation data.

At 16:30 on 09 05, the M/V Fred J. Agnich departed Marathon for the survey site. The streamer was deployed at 18:00, but weather conditions delayed the deployment of the airgun array until 04:00 the next day. The first reflection data line, line BB', was recorded between 13:42 on 09 06 and 02:15 on 09 07, using a 20-s record and a 50-m shotpoint interval.

During the last portion of Line BB', the streamer rode deep at approximately 16 m, so it was retrieved for further ballasting. Three problems complicated streamer ballasting at this point in the survey: the fresh water had a lower specific gravity than the normal sea water environment; the water temperatures gradually dropped, causing the streamer fluid to lower thus reducing cable buoyancy; and the low shooting speed (4.3 knots maximum) mandated by the 20-s records (30-fold data; 50-m shotpoint interval) forced the streamer's remote depth controllers to operate at the limits of their capability. Consequently during the next few days, various solutions were tried to assure the streamer remained with depth specifications.

Geophoto shot the 'BFLINK' line between Lines BB' and FF' during its line change to test streamer performance. This line was terminated at shotpoint #456 because a three-degree drop in water temperature rendered the cable uncontrollable, and it sank. The vessel increased its speed and the cable returned to specified depths within 15 minutes.

With client approval, Line FF' was started at 20:00 with a new shotpoint interval of 62.5 m (24-fold data) to accommodate the increased vessel speed. After approximately 25 km of data had been successfully collected in this manner, the vessel's speed was changed back to 4.3 knots, and the 50-m shotpoint interval was used once again to see if 30-fold data could be recorded. Shortly thereafter, the cable started to sink, so the crew returned to 24-fold data as of shotpoint #903.

A second attempt to return to 30-fold data was made at 10:15 on 09 08 at the start of the dogleg portion of Line F'F" as it appeared water temperatures had risen. Again just over 25 km of data were successfully recorded, but then the streamer started to sink. At shotpoint #2096, the fold was reduced to 24, the vessel speed was increased to 5 knots, and the shotpoint interval was changed to 62.5 m. The remainder of the survey was recorded in this manner.

After additional ballasting work was completed on the streamer, Line AA' was started at 09:50 on 09 09 and continued until the streamer sank too low the next day. The remainder of Line AA' was completed at 14:30, although the vessel stopped the end of the line 20 shotpoints early to avoid damaging the streamer in shallow water. After the client representative and a Geophoto field service representative were dispatched in the Zodiac boat for Jackfish, Ontario, the vessel retrieved its guns and headed for Line GG', which was recorded between 03:12 and 08:48 on 09 11. After the completion of this line, the vessel recorded data for another survey.

The M/V Fred J. Agnich resumed work on the GSC-USGS survey at 09:00 on 09 12 as the vessel headed for Line CC'. Failure of the CMS unit halted work on this line at 18:36. A portion of the line was reshot as part of Line CC'A (table 1), and all section of the line were completed by 06:08 on 09 13. The vessel then recorded data for another survey.

The M/V Fred J. Agnich renewed work on this program on 09 16 at 17:30 while at port at Sault Ste. Marie. The tasks of replenishing supplies and changing crew were completed at 02:30, and the vessel set a course for the

south end of Line 3 in Lake Michigan. After the streamer was reconfigured to accommodate shallow water, Line 3 was recorded between 13:06 on 09 18 and 11:42 on 09 19. An additional 67.5 km of data were recorded on a dogleg portion of this line. When the streamer was retrieved upon completion of this line, the cable caught on the propeller, damaging two sections. Repairs were effected while the vessel traveled to Lake Huron.

The vessel reached Lake Huron on 09 20. To accommodate the shallow water conditions, the streamer received additional isopar and floats before recording started on Line 1 at 19:43. Recording progressed smoothly on this line through the Mississagi Strait into the North Channel, until shallow water halted production at 07:00 the next day. The vessel then scouted shooting conditions while heading for the eastern end of Line 2A in Georgian Bay, and determined this line could be successfully recorded. Line 2A was started at 06:49 on 09 22. Recording progressed smoothly through the hazardous portion of the line between Georgian Bay and Lake Huron, and the line, which also had been increased in length at no additional charge, was successfully completed at 16:30 the next day. The airgun array and streamers were retrieved, and the crew set a course for Sarnia, Ontario, marking the completion of this survey.

#### STREAMER DETAILS

A 3024-m Texas Instruments streamer, comprised of 120 x 25 m groups, each containing 27 acceleration cancelling hydrophones, was towed at an average depth range of 10 m to 14 m to collect seismic data.

Streamer Type	Texas Instruments neutral bouyancy, continuous tow
Length (Center to Center)	3024 meters
Number of Live Sections	60
Live Section Length	50 m
Number of Groups	120
Group Length	25 m
Number of Hydrophones/Group	27
Hydrophone Interval	.93 meters
Type of Hydrophone	TI two chip dish
Depth Transducer Length	4 m
Compass Section Length	3 m
Front End Adapter	1 m
Length of Tailbuoy Rope	183 m
Stretch Section Length	50 m

## STREAMER DETAILS CONTINUED

Total length of nylon stretch sections	250 m
Stretch Factor	10% - 15%
Skin Type	PU (cold water skin)
Target Cable Depth	12 m (+/- 2 m)
Ship Speed during Production	4.3 - 5.3 knots
Average Water Temperature	12 Degrees Celsius
Type of Depth Controllers	RCL-2 Cable Levelers (individually programmable)

---

### SOURCE

A wide-tuned airgun array of 127.48 L capacity, comprised of 60 active guns with various characteristics towed on six buoy-supported strings, was used to generate seismic energy at 50 m and 62.5 m intervals. Compressed air at an operating pressure of approximately 13.8 MPa was supplied by three Sullair and four Chicago Pneumatic PBV-44-300 compressors. A GSI TIGER II\* timing controller assured precision firing of the individual airguns.

### AIRGUN DESCRIPTION

Type of Source	Six strings, staggered array
Type of Airguns	TI Mk. II & III Pnu-Con
Total Volume in Use	127.49 L
Total Spare Volume	34.58 L
Operating Depth	12 meters +/- 1 meter
Timing Controller	
Type	TIGER II*
Serial No.	04
Firing Delay	51.2 ms
Compressors	
Type	Sullair
No. in Use	3
Type	GMC/Dual PB44-300
No. in Use	4

AIRGUN DESCRIPTION CONTINUED

Coalescing Gun Separation Distance	.53 m
Array Width	80 m +/- 1 m
Gun String Length	9.9 m
Distance, Stern to First Gun	
Inner Arrays	65 m
Middle Arrays	70 m
Outer Arrays	75 m
Distance, Stern to Gun Array Centre	73.3 m
Distance, Common Navigation Position to Acoustic Centre of Gun Array	74.0 m
Distance, Array Centre to Near Group Centre (OFFSET)	288 m - 236 m

\*Trademark of Geophysical Service Inc.

APPENDIX B. SUMMARY OF THE GLIMPCE MULTICHANNEL REFLECTION DATA

The purpose of this appendix is to correlate the original line names to the ones chosen for the final displays and to allow future users of the data to correlate shotpoint information with archived demultiplexed tapes.

<u>Lake</u>	<u>GSI Line Name</u>	<u>GLIMPCE Line Name</u>
Superior	A'A (part 1)	A
	A'A (part 2)	A
	BB	B
	CC'	C
	CC'(A)	C
	BFLINK	F
	FF'	F
	F'F''	F
	GG	G
	Michigan	3
Huron	1	I
	2A	J

The shot numbers in the following table are sequential numbers put into the trace headers by the DISCO demultiplexing program. Due to missed shot points, these numbers may not correspond directly to actual shotpoint locations. However, they generally are within  $\pm 500$  meters of the actual shotpoint locations. The original record identification numbers (FF ids) are still in the headers and users can always correlate these with exact shotpoint locations using the field observer's notes.

The archived demultiplexed tapes are recorded using DISCO's VAX internal format with a packing density of 6,250 bits per inch. The traces are twenty (20) seconds long with a sampling interval of four (4) ms resulting in 5,000 samples per trace. The recorded ensembles are in shot order with channel numbers in the trace headers and with channel number 120 being the near trace.

Explanation for the following pages:

Lake: The lake where the line was shot  
 Line: The original line name  
 Reel: The number of the demultiplexed reel archived in Denver Processing Center for the USGS  
 F-Shot: The number of the first shot occurring on the reel  
 F-Trace: The number of the first channel number within the first shot  
 L-Shot: The number of the last shot occurring on the reel  
 L-Trace: The number of the last channel number within the last shot

LAKE	LINE	REEL	F-SHOT	F-TRACE	L-SHOT	L-TRACE
SUPERIOR	A'A1	19116	100	1	167	106
SUPERIOR	A'A1	19117	167	107	219	96
SUPERIOR	A'A1	19118	219	97	287	113
SUPERIOR	A'A1	19119	287	114	356	8
SUPERIOR	A'A1	19120	356	9	424	15
SUPERIOR	A'A1	19121	424	16	472	78
SUPERIOR	A'A1	19122	472	79	532	2
SUPERIOR	A'A1	19123	532	3	591	46
SUPERIOR	A'A1	19124	591	47	657	97
SUPERIOR	A'A1	19125	657	98	711	120
SUPERIOR	A'A1	19126	706	1	772	110
SUPERIOR	A'A1	19127	772	111	839	75
SUPERIOR	A'A1	19128	839	76	907	111
SUPERIOR	A'A1	19129	907	112	976	51
SUPERIOR	A'A1	19130	976	52	1044	69
SUPERIOR	A'A1	19131	1044	70	1112	101
SUPERIOR	A'A1	19132	1112	102	1181	15
SUPERIOR	A'A1	19133	1181	16	1249	77
SUPERIOR	A'A1	19134	1249	78	1316	54
SUPERIOR	A'A1	19135	1316	55	1381	62
SUPERIOR	A'A1	19136	1381	63	1448	9
SUPERIOR	A'A1	19137	1448	10	1516	87
SUPERIOR	A'A1	19138	1516	88	1578	87
SUPERIOR	A'A1	19139	1578	88	1645	21
SUPERIOR	A'A1	19140	1645	22	1713	54
SUPERIOR	A'A1	19141	1713	55	1770	120
SUPERIOR	A'A1	19142	1771	1	1839	30
SUPERIOR	A'A1	19143	1839	31	1906	119
SUPERIOR	A'A1	19144	1906	120	1975	29
SUPERIOR	A'A1	19145	1975	30	2043	68
SUPERIOR	A'A1	19146	2043	69	2111	75
SUPERIOR	A'A1	19147	2111	76	2179	57
SUPERIOR	A'A1	19148	2179	58	2247	4
SUPERIOR	A'A1	19149	2247	5	2314	99
SUPERIOR	A'A1	19150	2314	100	2370	108
SUPERIOR	A'A1	19151	2370	109	2372	120
SUPERIOR	A'A2	19152	2289	1	2355	82
SUPERIOR	A'A2	19153	2355	83	2415	114
SUPERIOR	A'A2	19154	2415	115	2484	33
SUPERIOR	A'A2	19155	2484	34	2552	48
SUPERIOR	A'A2	19156	2552	49	2620	34
SUPERIOR	A'A2	19157	2620	35	2688	42
SUPERIOR	A'A2	19158	2688	43	2756	55
SUPERIOR	A'A2	19159	2756	56	2825	16
SUPERIOR	A'A2	19160	2825	17	2893	2
SUPERIOR	A'A2	19161	2893	3	2961	7
SUPERIOR	A'A2	19162	2961	8	3028	33
SUPERIOR	A'A2	19163	3028	34	3097	60
SUPERIOR	A'A2	19164	3097	61	3101	113
SUPERIOR	A'A2	19165	3101	114	3170	1
SUPERIOR	A'A2	19166	3170	2	3238	117
SUPERIOR	A'A2	19167	3238	118	3307	67
SUPERIOR	A'A2	19168	3307	68	3375	17

LAKE	LINE	REEL	F-SHOT	F-TRACE	L-SHOT	L-TRACE
SUPERIOR	A'A2	19169	3375	18	3419	22
SUPERIOR	A'A2	19170	3419	23	3487	64
SUPERIOR	A'A2	19171	3487	65	3554	61
SUPERIOR	A'A2	19172	3554	62	3621	110
SUPERIOR	A'A2	19173	3621	111	3689	87
SUPERIOR	A'A2	19174	3689	88	3756	101
SUPERIOR	A'A2	19175	3756	102	3825	90
SUPERIOR	A'A2	19176	3825	91	3894	64
SUPERIOR	A'A2	19177	3894	65	3940	120
SUPERIOR	BB	19194	101	1	169	51
SUPERIOR	BB	19195	169	52	236	98
SUPERIOR	BB	19196	236	99	304	24
SUPERIOR	BB	19197	304	25	371	120
SUPERIOR	BB	19198	372	1	439	88
SUPERIOR	BB	19199	439	89	508	86
SUPERIOR	BB	19200	508	87	576	38
SUPERIOR	BB	19201	576	39	624	120
SUPERIOR	BB	19202	625	1	693	120
SUPERIOR	BB	19203	694	1	763	30
SUPERIOR	BB	19204	763	31	769	82
SUPERIOR	BB	19205	769	83	837	64
SUPERIOR	BB	19206	837	65	905	67
SUPERIOR	BB	19207	905	68	974	57
SUPERIOR	BB	19208	974	58	979	120
SUPERIOR	BB	19209	980	1	1048	52
SUPERIOR	BB	19210	1048	53	1115	55
SUPERIOR	BB	19211	1115	56	1183	105
SUPERIOR	BB	19212	1183	106	1250	74
SUPERIOR	BB	19213	1250	75	1319	13
SUPERIOR	BB	19214	1319	14	1387	26
SUPERIOR	BB	19215	1387	27	1455	114
SUPERIOR	BB	19216	1455	115	1522	87
SUPERIOR	BB	19217	1522	88	1591	73
SUPERIOR	BB	19218	1591	74	1659	91
SUPERIOR	BB	19219	1659	92	1728	29
SUPERIOR	BB	19220	1728	30	1797	13
SUPERIOR	BB	19221	1797	14	1865	91
SUPERIOR	BB	19222	1865	92	1932	88
SUPERIOR	BB	19223	1932	89	2001	50
SUPERIOR	BB	19224	2001	51	2038	120
SUPERIOR	CC'	19370	101	1	169	42
SUPERIOR	CC'	19371	169	43	227	110
SUPERIOR	CC'	19372	227	111	296	41
SUPERIOR	CC'	19373	296	42	365	4
SUPERIOR	CC'	19374	365	5	433	84
SUPERIOR	CC'	19375	433	85	491	72
SUPERIOR	CC'	19376	491	73	558	68
SUPERIOR	CC'	19377	558	69	625	57
SUPERIOR	CC'	19378	625	58	692	11
SUPERIOR	CC'	19379	692	12	750	78
SUPERIOR	CC'	19380	750	79	818	67
SUPERIOR	CC'	19381	818	68	886	3
SUPERIOR	CC'	19382	886	4	907	31

LAKE	LINE	REEL	F-SHOT	F-TRACE	L-SHOT	L-TRACE
-----	-----	-----	-----	-----	-----	-----
SUPERIOR	CC'	19383	907	32	974	40
SUPERIOR	CC'	19384	974	41	978	120
SUPERIOR	CC'A	19385	741	1	741	36
SUPERIOR	CC'A	19386	741	37	808	15
SUPERIOR	CC'A	19387	808	16	874	33
SUPERIOR	CC'A	19388	874	34	941	10
SUPERIOR	CC'A	19389	941	11	1009	17
SUPERIOR	CC'A	19390	1009	18	1024	120
SUPERIOR	CC'A	19391	1025	1	1090	45
SUPERIOR	CC'A	19392	1090	46	1158	52
SUPERIOR	CC'A	19393	1158	53	1225	9
SUPERIOR	CC'A	19394	1225	10	1291	78
SUPERIOR	CC'A	19395	1291	79	1358	26
SUPERIOR	CC'A	19396	1358	27	1424	119
SUPERIOR	CC'A	19397	1424	120	1491	75
SUPERIOR	CC'A	19398	1491	76	1558	46
SUPERIOR	CC'A	19399	1558	47	1617	13
SUPERIOR	CC'A	19400	1617	14	1679	78
SUPERIOR	CC'A	19401	1679	79	1746	67
SUPERIOR	CC'A	19402	1746	68	1813	30
SUPERIOR	CC'A	19403	1813	31	1880	120
SUPERIOR	BFLINK	19479	101	1	167	80
SUPERIOR	BFLINK	19480	167	81	234	42
SUPERIOR	BFLINK	19481	234	43	301	102
SUPERIOR	BFLINK	19482	301	103	366	105
SUPERIOR	BFLINK	19483	366	106	434	49
SUPERIOR	BFLINK	19484	434	50	441	120
SUPERIOR	FF'	19307	457	1	524	55
SUPERIOR	FF'	19308	524	56	592	11
SUPERIOR	FF'	19309	592	12	658	79
SUPERIOR	FF'	19310	658	80	726	17
SUPERIOR	FF'	13911	726	18	793	66
SUPERIOR	FF'	19312	793	67	861	60
SUPERIOR	FF'	19313	861	61	918	120
SUPERIOR	FF'	19314	919	1	988	14
SUPERIOR	FF'	19315	988	15	1056	111
SUPERIOR	FF'	19316	1056	112	1123	108
SUPERIOR	FF'	19317	1123	109	1190	69
SUPERIOR	FF'	19318	1190	70	1257	72
SUPERIOR	FF'	19319	1257	73	1326	69
SUPERIOR	FF'	19320	1326	70	1395	17
SUPERIOR	FF'	19321	1395	18	1464	2
SUPERIOR	FF'	19322	1464	3	1532	65
SUPERIOR	FF'	19323	1532	66	1572	120
SUPERIOR	F'F"	19324	101	1	169	33
SUPERIOR	F'F"	19325	169	34	238	17
SUPERIOR	F'F"	19326	238	18	306	43
SUPERIOR	F'F"	19328	374	92	442	90
SUPERIOR	F'F"	19329	442	91	510	101
SUPERIOR	F'F"	19330	510	102	576	16
SUPERIOR	F'F"	19331	576	17	643	72
SUPERIOR	F'F"	19332	643	73	703	120
SUPERIOR	F'F"	19333	704	1	768	60

LAKE	LINE	REEL	F-SHOT	F-TRACE	L-SHOT	L-TRACE
SUPERIOR	F'F"	19334	768	61	836	18
SUPERIOR	F'F"	19335	836	19	903	41
SUPERIOR	F'F"	19336	903	42	971	46
SUPERIOR	F'F"	19337	971	47	1036	30
SUPERIOR	F'F"	19338	1036	31	1103	58
SUPERIOR	F'F"	19339	1103	59	1169	12
SUPERIOR	F'F"	19340	1169	13	1237	6
SUPERIOR	F'F"	19341	1237	7	1302	73
SUPERIOR	F'F"	19342	1302	74	1352	120
SUPERIOR	GG	19178	101	1	168	88
SUPERIOR	GG	19179	168	89	236	35
SUPERIOR	GG	19180	236	36	301	59
SUPERIOR	GG	19181	301	60	368	117
SUPERIOR	GG	19182	368	118	433	27
SUPERIOR	GG	19183	433	28	501	41
SUPERIOR	GG	19184	501	42	569	1
SUPERIOR	GG	19185	569	2	636	41
SUPERIOR	GG	19186	636	42	692	52
SUPERIOR	GG	19187	692	53	760	103
SUPERIOR	GG	19188	760	104	830	30
SUPERIOR	GG	19189	830	31	895	94
SUPERIOR	GG	19190	895	95	954	2
SUPERIOR	GG	19191	954	3	962	120
MICHIGAN	3	19404	101	1	169	91
MICHIGAN	3	19405	169	92	236	97
MICHIGAN	3	19406	236	98	302	1
MICHIGAN	3	19407	302	2	370	47
MICHIGAN	3	19408	370	48	437	72
MICHIGAN	3	19409	437	73	504	26
MICHIGAN	3	19410	504	27	572	102
MICHIGAN	3	19411	572	103	639	107
MICHIGAN	3	19412	639	108	706	28
MICHIGAN	3	19413	706	29	773	78
MICHIGAN	3	19414	773	79	840	73
MICHIGAN	3	19415	840	74	908	57
MICHIGAN	3	19416	908	58	975	91
MICHIGAN	3	19417	975	92	1040	94
MICHIGAN	3	19418	1040	95	1106	47
MICHIGAN	3	19419	1106	48	1174	82
MICHIGAN	3	19420	1174	83	1242	99
MICHIGAN	3	19421	1242	100	1310	107
MICHIGAN	3	19422	1310	108	1377	66
MICHIGAN	3	19423	1377	67	1445	79
MICHIGAN	3	19424	1445	80	1467	120
MICHIGAN	3	19425	1468	1	1535	6
MICHIGAN	3	19426	1535	7	1602	115
MICHIGAN	3	19427	1602	116	1657	120
MICHIGAN	3	19428	1658	1	1725	35
MICHIGAN	3	19429	1725	36	1758	120
MICHIGAN	3	19430	1759	1	1808	120
MICHIGAN	3	19431	1809	1	1844	120
MICHIGAN	3	19432	1845	1	1911	42
MICHIGAN	3	19433	1911	43	1978	72

LAKE	LINE	REEL	F-SHOT	F-TRACE	L-SHOT	L-TRACE
MICHIGAN	3	19434	1978	73	2046	52
MICHIGAN	3	19435	2046	53	2090	120
MICHIGAN	3	19436	2091	1	2155	107
MICHIGAN	3	19437	2155	108	2222	120
MICHIGAN	3	19438	2223	1	2290	33
MICHIGAN	3	19439	2290	34	2358	6
MICHIGAN	3	19440	2358	7	2424	74
MICHIGAN	3	19441	2424	75	2488	117
MICHIGAN	3	19442	2488	118	2503	97
MICHIGAN	3	19443	2503	98	2569	94
MICHIGAN	3	19444	2569	95	2637	26
MICHIGAN	3	19445	2637	27	2651	3
MICHIGAN	3	19446	2651	4	2718	110
MICHIGAN	3	19447	2718	111	2720	2
MICHIGAN	3	19448	2720	3	2786	33
MICHIGAN	3	19449	2786	34	2839	120
MICHIGAN	3	19450	2840	1	2856	120
MICHIGAN	3	19451	2857	1	2924	6
MICHIGAN	3	19452	2924	7	2992	34
MICHIGAN	3	19453	2992	35	3029	120
MICHIGAN	3	19454	3030	1	3098	4
MICHIGAN	3	19455	3098	5	3166	12
MICHIGAN	3	19456	3166	13	3233	95
MICHIGAN	3	19457	3233	96	3301	81
MICHIGAN	3	19458	3301	82	3368	30
MICHIGAN	3	19459	3368	31	3435	62
MICHIGAN	3	19460	3435	63	3503	38
MICHIGAN	3	19461	3503	39	3571	61
MICHIGAN	3	19462	3571	62	3585	120
MICHIGAN	3	19463	3586	1	3651	56
MICHIGAN	3	19464	3651	57	3719	75
MICHIGAN	3	19465	3719	76	3788	5
MICHIGAN	3	19466	3788	6	3855	107
MICHIGAN	3	19467	3855	108	3922	115
MICHIGAN	3	19468	3922	116	3988	46
MICHIGAN	3	19469	3988	47	4056	61
MICHIGAN	3	19470	4056	62	4124	38
MICHIGAN	3	19471	4124	39	4191	75
MICHIGAN	3	19472	4191	76	4259	22
MICHIGAN	3	19473	4259	23	4327	6
MICHIGAN	3	19474	4327	7	4393	94
MICHIGAN	3	19475	4393	95	4460	59
MICHIGAN	3	19476	4460	60	4527	83
MICHIGAN	3	19477	4527	84	4595	21
MICHIGAN	3	19478	4595	22	4616	120
MICHIGAN	3	19404	4435	1	4503	20
MICHIGAN	3	19405	4503	21	4571	69
MICHIGAN	3	19406	4571	70	4637	109
MICHIGAN	3	19407	4637	110	4706	29
MICHIGAN	3	19408	4706	30	4774	2
MICHIGAN	3	19409	4774	3	4842	29
MICHIGAN	3	19410	4842	30	4909	73
MICHIGAN	3	19411	4909	74	4949	14

LAKE	LINE	REEL	F-SHOT	F-TRACE	L-SHOT	L-TRACE
MICHIGAN	3	19412	4949	15	5015	107
MICHIGAN	3	19413	5015	108	5026	120
MICHIGAN	3	19296	1759	1	1768	120
HURON	1	19343	101	1	168	60
HURON	1	19344	168	61	235	114
HURON	1	19345	235	115	302	6
HURON	1	19346	302	7	369	115
HURON	1	19347	369	116	437	75
HURON	1	19348	437	76	502	112
HURON	1	19349	502	113	570	43
HURON	1	19350	570	44	636	117
HURON	1	19351	636	118	703	120
HURON	1	19352	704	1	772	94
HURON	1	19353	772	95	812	120
HURON	1	19354	813	1	880	60
HURON	1	19355	880	61	947	60
HURON	1	19356	947	61	1014	99
HURON	1	19357	1014	100	1082	116
HURON	1	19358	1082	117	1149	80
HURON	1	19359	1149	81	1190	120
HURON	1	19360	1191	1	1259	60
HURON	1	19361	1259	61	1326	61
HURON	1	19362	1326	62	1394	103
HURON	1	19363	1394	104	1463	28
HURON	1	19364	1463	29	1530	51
HURON	1	19365	1530	52	1598	55
HURON	1	19366	1598	56	1665	91
HURON	1	19367	1665	92	1733	100
HURON	1	19368	1733	101	1800	77
HURON	1	19369	1800	78	1820	120
HURON	2A	19225	101	1	168	110
HURON	2A	19226	168	111	235	98
HURON	2A	19227	235	99	303	110
HURON	2A	19228	303	111	371	104
HURON	2A	19229	371	105	440	38
HURON	2A	19230	440	39	501	120
HURON	2A	19231	502	1	570	81
HURON	2A	19232	570	82	638	117
HURON	2A	19233	638	118	707	5
HURON	2A	19234	707	6	774	82
HURON	2A	19235	774	83	842	33
HURON	2A	19236	842	34	910	61
HURON	2A	19237	910	62	979	23
HURON	2A	19238	979	24	1047	80
HURON	2A	19239	1047	81	1115	110
HURON	2A	19240	1115	111	1184	87
HURON	2A	19241	1184	88	1251	61
HURON	2A	19242	1251	62	1319	75
HURON	2A	19243	1319	76	1386	20
HURON	2A	19244	1386	21	1452	115
HURON	2A	19245	1452	116	1460	120
HURON	2A	19246	1461	1	1527	82
HURON	2A	19247	1527	83	1595	77

LAKE	LINE	REEL	F-SHOT	F-TRACE	L-SHOT	L-TRACE
HURON	2A	19248	1595	78	1662	67
HURON	2A	19249	1662	68	1726	21
HURON	2A	19250	1726	22	1794	119
HURON	2A	19251	1794	120	1801	120
HURON	2A	19252	1802	1	1841	60
HURON	2A	19253	1841	61	1908	77
HURON	2A	19254	1908	78	1977	31
HURON	2A	19255	1977	32	2044	69
HURON	2A	19256	2044	70	2112	111
HURON	2A	19257	2112	112	2179	95
HURON	2A	19258	2179	96	2248	4
HURON	2A	19259	2248	5	2314	111
HURON	2A	19260	2314	112	2382	3
HURON	2A	19261	2382	4	2450	63
HURON	2A	19262	2450	64	2517	44
HURON	2A	19263	2517	45	2585	57
HURON	2A	19264	2585	58	2653	80
HURON	2A	19265	2653	81	2688	120
HURON	2A	19266	2689	1	2757	32
HURON	2A	19267	2757	33	2825	113
HURON	2A	19268	2825	114	2894	47
HURON	2A	19269	2894	48	2962	86
HURON	2A	19270	2962	87	3029	99
HURON	2A	19271	3029	100	3098	11
HURON	2A	19272	3098	12	3166	43
HURON	2A	19273	3166	44	3234	92
HURON	2A	19274	3234	93	3300	120
HURON	2A	19275	3301	1	3369	41
HURON	2A	19276	3369	42	3437	82
HURON	2A	19277	3437	83	3505	103
HURON	2A	19278	3505	104	3575	10
HURON	2A	19279	3575	11	3642	89
HURON	2A	19280	3642	90	3708	85
HURON	2A	19281	3708	86	3776	114
HURON	2A	19282	3776	115	3844	3
HURON	2A	19283	3844	4	3911	27
HURON	2A	19284	3911	28	3979	68
HURON	2A	19285	3979	69	4048	41
HURON	2A	19286	4048	42	4115	120
HURON	2A	19287	4116	1	4184	58
HURON	2A	19288	4184	59	4253	26
HURON	2A	19289	4253	27	4314	120
HURON	2A	19290	4315	1	4382	32
HURON	2A	19291	4382	33	4434	120
HURON	2A	19292	4435	1	4503	20
HURON	2A	19293	4503	21	4570	110
HURON	2A	19294	4570	111	4636	97
HURON	2A	19295	4636	98	4704	65
HURON	2A	19297	4704	66	4772	117
HURON	2A	19298	4772	118	4839	120
HURON	2A	19299	4840	1	4907	67
HURON	2A	19301	4907	68	4974	31
HURON	2A	19302	4974	32	5041	14

LAKE	LINE	REEL	F-SHOT	F-TRACE	L-SHOT	L-TRACE
HURON	2A	19303	5041	15	5106	10
HURON	2A	19304	5106	11	5172	103
HURON	2A	19305	5172	104	5241	99
HURON	2A	19306	5241	100	5255	120